haematologica
Journal of The Ferrata Storti Foundation

Aging-induced pseudouridine synthase 10 impairs hematopoietic stem cells

by Yuqian Wang, Zhenzhen Zhang, Hanqing He, Jinghui Song, Yang Cui, Yunan Chen, Yuan Zhuang, Xiaoting Zhang, Mo Li, Xinxiang Zhang, Michael Q. Zhang, Minglei Shi, Chengqi Yi, and Jianwei Wang

Received: October 4, 2022.
Accepted: May 4, 2023.

Citation: Yuqian Wang, Zhenzhen Zhang, Hanqing He, Jinghui Song, Yang Cui, Yunan Chen, Yuan Zhuang, Xiaoting Zhang, Mo Li, Xinxiang Zhang, Michael Q. Zhang, Minglei Shi, Chengqi Yi, and Jianwei Wang. Aging-induced pseudouridine synthase 10 impairs hematopoietic stem cells. Haematologica. 2023 May 11. doi: 10.3324/haematol.2022.282211 [Epub ahead of print]

Aging-induced pseudouridine synthase 10 impairs hematopoietic stem cells

Yuqian Wang[1*], Zhenzhen Zhang[2*], Hanqing He[1], Jinghui Song[3], Yang Cui[1], Yunan Chen[4], Yuan Zhuang[5], Xiaoting Zhang[5], Mo Li[6], Xinxiang Zhang[4], Michael Q. Zhang[2 7 8#], Minglei Shi[2#], Chengqi Yi[5#], Jianwei Wang[1#]

[1]School of Pharmaceutical Sciences, Tsinghua University, Beijing 100084, China.

[2]School of Medicine, Tsinghua University, Beijing 100084, China.

[3]Department of Bioengineering, University of California San Diego, La Jolla, CA 92093, USA.

[4]Beijing National Laboratory for Molecular Sciences, Key Laboratory of Bioorganic Chemistry and Molecular Engineering of Ministry of Education, College of Chemistry and Molecular Engineering, Peking University, Beijing, China.

[5]Department of Basic Medical Sciences, School of Medicine, Institute for Immunology, Beijing Key Lab for Immunological Research on Chronic Diseases, THU-PKU Center for Life Sciences, Tsinghua University, Beijing, China.

[6]Center for Reproductive Medicine, Department of Obstetrics and Gynecology, Peking University Third Hospital, Beijing, 100191, China.

[7]MOE Key Laboratory of Bioinformatics; Bioinformatics Division and Center for Synthetic & Systems Biology, BNRist; Department of Automation, Tsinghua University, Beijing 100084, China.

[8]Department of Biological Sciences, Center for Systems Biology, the University of Texas, Richardson, TX 75080-3021, USA.

[*]These authors contribute equally

[#]Correspondence: michael.zhang@utdallas.edu; shiml79@tsinghua.edu.cn; chengqi.yi@pku.edu.cn; jianweiwang@mail.tsinghua.edu.cn; wangjianwei@ihcams.ac.cn

Authorship Contribution

Conceptualization, J.W. and C.Y.; Methodology, J.W. and C.Y.; Investigation, Y.W., Z.Z., H.H., J.S., Y.C, Y.C., Y.Z. and X.Z.; Formal Analysis, J.W., C.Y., M.S., M.Q.Z., X.Z. and M.L.; Resources, J.W., C.Y., M.S. and M.Q.Z.; Writing, J.W. and C.Y.; Funding Acquisition, J.W. and C.Y.; Supervision, J.W., C.Y., M.S. and M.Q.Z.

Declaration of interests

The authors declare no competing interests.

Acknowledgments

We thank the Tsinghua-Peking Center for Life Sciences for facility and financial support. This work was supported by grant numbers Z200022, 82250002, 81870118 and 2018YFA0800200 to J.W.W., and 2019YFA0110900, 2019YFA0802200 to C.Q.Y, and 81890991 to M.S. from the National Key R&D Program of China or the Beijing Municipal Science & Technology Commission and the National Natural Science Foundation of China.

Data-sharing statement

The data are available on request from the first author.

ABSTRACT

Aged hematopoietic stem cells (HSCs) exhibit compromised reconstitution capacity and differentiation-bias towards myeloid lineage. While, the molecular mechanism behind it remains not fully understood. In this study, we observed that the expression of pseudouridine (Ψ) synthase 10 is increased in aged hematopoietic stem and progenitor cells (HSPCs) and enforced PUS10 recapitulates the phenotype of aged HSCs, which is not achieved by its Ψ synthase activity. Consistently, we observed no difference of tRNA pseudouridylation profile between young and aged HSPCs. No significant alteration of hematopoietic homeostasis and HSC function is observed in young *Pus10*$^{-/-}$ mice, while aged *Pus10*$^{-/-}$ mice exhibit mild alteration of hematopoietic homeostasis and HSC function. Moreover, we observed that PUS10 is ubiquitinated by E3 ubiquitin ligase CRL4^{DCAF1} complex and the increase of PUS10 in aged HSPCs is due to aging-declined CRL4^{DCAF1}-mediated ubiquitination degradation signaling. Taken together, this study for the first time evaluated the role of PUS10 in HSC aging and function, and provided novel insight for HSC rejuvenation and clinical application.

INTRODUCTION

Hematopoietic stem cell (HSC) generates all of the blood cells throughout life-span [1, 2]. During aging, the function of HSCs declines, featured as compromised reconstitution capacity and differentiation skewing towards myeloid lineage [3, 4]. Although previous studies have identified various molecular signaling promoting HSC aging [5-8] , the exact molecular mechanism is still not fully understood.

It has been known for several decades that more than 170 different types of chemical modifications to RNA exist [9]. Pseudouridine (Ψ), known as "the fifth nucleotide" in RNA, was first identified in 1951 and is the most abundant post-transcriptional RNA modification (with an estimated c/U ratio of 7–9%) [10-12]. Ψ is generated from isomerization of uridine, which is catalyzed by Ψ synthases [13-15]. Ψ plays important role in various aspects of RNA biology, and therefore participates in many biological process, including translational control [16, 17], RNA folding [18-22], protein translation [23-26], and clinical diseases [27-32]. A recent study revealed that dysfunction of PUS7 blocks the differentiation of HSCs due to the lack of pseudouridylation of mTOG tRFs [16]. Moreover, the expression of PUS7 is decreased in hematopoietic stem and progenitor cells (HSPCs) of patients with myelodysplastic syndrome and delivery of pseudouridylated mTOGs to HSPCs of myelodysplastic syndromes patients improves their colony formation capacity and differentiation potential [33]. In addition, DKC1 is required for accurate HSC differentiation and maintenance of HSC function [34, 35]. The above studies reveal the importance of Ψ in modulating HSC differentiation and malignancies, while whether Ψ participates in HSC aging has never been investigated.

In this study, we observed that the protein of Ψ synthase 10 (PUS10) is increased in aged HSPCs. By conducting *in vivo* functional assay, we observed that enforced PUS10 impairs the reconstitution capacity of HSPCs, which is independent on their Ψ synthase activity. By profiling the Ψ landscape in HSPCs, we observed no difference of Ψ between young and aged HSPCs at detectable locations. Moreover, we observed that PUS10 interacts with E3 ubiquitin ligase $CRL4^{DCAF1}$ complex and is ubiquitinated by this complex. Aging-declined $CRL4^{DCAF1}$ results in the accumulation

of PUS10 in HSPCs. Taken together, this study for the first time elucidated the role of PUS10 in HSC aging and function, and provided novel insight for HSC rejuvenation and clinical application.

METHODS

Mice

C57BL/6 mice (CD45.2), C57BL/6-SJL (CD45.1) mice were from the Jackson Laboratory. *Pus10*$^{-/-}$ mice were kindly provided by Dr. Mo Li, Peking University Third Hospital, Beijing. *Pus10*$^{-/-}$ mice on C57BL/6N background were generated by deleting the 2nd exon using CRISPR-Cas9 system. The gRNAs used to generate *Pus10*$^{-/-}$ mice were listed in Table S2. The genotyping primers were listed in Table S3. The recipient mice (CD45.1/2) in the competitive transplantation assays were the first generation of C57BL/6 (CD45.2) and B6.SJL (CD45.1) mice. All mice were housed in specific pathogen-free conditions. All procedures were approved by the Institutional Animal Care and Use Committee (IACUC) of Tsinghua University.

Small RNA DM–Ψ-seq

Small RNA (<200nt) was extracted and purified using miRNeasy Mini Kit (Qiagen) and RNeasy MinElute Cleanup Kit (Qiagen). Purified small RNA fragments were demethylated by wild-type and mutant AlkBs, purified by phenol/chloroform extraction and ethanol precipitation, labeled by CMC. The demethylation reaction and CMC labeling were performed as described [14]. Briefly, 50ng small RNA was denatured at 65 °C for 5 min and demethylated by wild-type and D135S mutant AlkBs. The purified small RNA was denatured at 80 °C for 5 min, added to BEU buffer with or without CMC, incubated at 37 °C for 20 min, then purified by ethanol precipitation.The purified RNA was dissolved in sodium carbonate buffer and shaked at 37 °C for 6 h. The library was established as described [14, 36] . Briefly, the small RNA was dephosphorylated with CIP (NEB). The 3' adaptor ligation was added with T4 RNA ligase2, truncated KQ (NEB), followed by 5' Deadenylase (NEB) and RecJf (NEB) digestion. The RNA was reverse transcribed by SuperScript III reverse transcriptase (Invitrogen), then digested by RNase H. The 5' adaptor ligation was

added with T4 RNA ligase 1, high concentration (NEB). The ligated cDNA was amplified by Q5 High-Fidelity 2× Master Mix (NEB). The purified libraries were sequenced on Illumina NovaSeq 6000.

Identification of pseudouridine sites and levels on tRNA

For tRNA DM-Ψ-seq data, the analysis was performed as described before [14, 36] . Briefly, the adapter sequences of reads 2 were trimmed with Trim-galore v0.6.5 (parameters: -q 20--phred33--length 25-e 0.1--stringency 3). PCR duplication was removed with Fastx_toolkit v0.0.14 before discarding the random barcode in the 5' end. Processed reads were further mapped to the genomic tRNA sequences from GtRNAdb atabase (http://gtrnadb.ucsc.edu/genomes/eukaryota/Mmusc10/) with Bowtie2 v2.3.5 (parameters: bowtie-a--best--strata--chunkmbs 2000). To identify the pseudouridine sites of tRNA, the following criteria were considered: (1) the pseudouridine sites appearing in all independent replicates; (2) stop rate<1% in the BEU sample; (3) CMC coverage>50; (4) stop reads number>5 in the CMC sample; (5) stop rate (CMC−BEU) difference>4%; (6) Fisher test adjusted P value <0.05. Finally, the pseudouridine level change for tRNA between young and old HSPCs was evaluated and visualized via R package ggplot2.

Statistical analysis

Data are shown as mean ± SD. Student's t test (Two-tailed unpaired) was used for comparisons between the groups using GraphPad Prism 6.0 software.

Author Declarations

The approval by the IRB and/or ethics committee has been obtained.

RESULTS

PUS10 is increased in aged HSPCs

Due to the scarcity of HSCs, we purified HSPCs by using the combination of $CD48^{-}$LSK ($cKit^{+}$ $Sca1^{+}$ Lin^{-}) according to previous reports [37-39]. The protein of PUS10 between young and aged HSPCs was examined by western blot and it showed that PUS10 is increased upon aging (Fig. 1A and B). To further confirm this result, we investigated the expression of PUS10 in a database, wherein the researchers compared

the proteomic profile between young and aged HSCs ($CD34^-CD150^+Flt3^-$ LSK) [40]. The result shows that PUS10 is indeed increased in aged HSCs (Fig. 1C).

Enforced PUS10 impairs the reconstitution capacity of HSPCs

To further investigate whether the increase of PUS10 plays a functional role on HSCs, we cloned the cDNA of mouse *Pus10* into a lentiviral vector [3], and it exhibited efficient overexpression of PUS10 (Suppl. Fig. 1A and B). Freshly isolated WT LSK cells were infected by PUS10-carrying lentivirus. 72 hours later, 2×10^4 GFP^+ cells were purified and transplanted into lethally irradiated recipients together with 2×10^5 competitor cells (Fig. 1D). Chimera in peripheral blood was evaluated every four weeks until the 12^{th} week by using this gating strategy (Suppl. Fig. 1C and D). The results showed that enforced PUS10 severely impairs the reconstitution capacity of HSPCs (Fig. 1E). Moreover, enforced PUS10 promotes HSPC differentiation bias towards myeloid lineage (Fig. 1F), which is a classical phenomenon of aged HSCs. Consistently, enforced PUS10 significantly inhibits HSPC expansion *in vitro* (Fig. 1G and H).

To investigate whether the inhibitory function of enforced PUS10 on HSPCs depends on its Ψ catalytic activity, we mutated the key enzyme site of PUS10 to generate catalytic dead $PUS10^{D342A}$ according to a previous study[14]. We firstly measured the Ψ/U ratio in WT and *Pus10*$^{-/-}$ $lineage^-cKit^+$ (LK) cells using liquid chromatography-tandem mass spectrometry (LC-MS/MS). The result showed that targeted dysfunction of *Pus10* leads to significant decrease of the Ψ/U ratio. To test whether $PUS10^{D342A}$ is an inactive Ψ synthase, we reintroduced wild-type PUS10 and $PUS10^{D342A}$ into *Pus10*$^{-/-}$ LK cells, and measured the Ψ/U ratio for them. The result showed that the decrease of the Ψ/U ratio upon *Pus10* deletion is rescued by the reintroduction of wild-type PUS10, but not $PUS10^{D342A}$ (Fig. 1I). This result indicates that D342 residue is the key enzyme site for its Ψ synthase activity.

To investigate whether the Ψ synthase activity of PUS10 modulates HSC aging, freshly isolated WT LSK cells were infected by either PUS10 or $PUS10^{D342A}$-overexpressing lentivirus for 72 hours, and 2×10^4 GFP^+ cells were

transplanted into lethally irradiated recipients together with 2×10^5 competitor cells. The chimera in peripheral blood was evaluated every four weeks until the 12^{th} week. The results revealed that both enforced PUS10 and $PUS10^{D342A}$ significantly impair the reconstitution capacity of HSPCs (Fig. 1J), indicating that the destructive role of PUS10 on HSPCs is independent on its enzymatic activity.

No difference of pseudouridylation profile between young and aged HSPCs

We then sought out to investigate whether aged HSCs exhibit aberrant Ψ profile compared to young ones. Due to the limited cell number of HSCs and a large amount of cells are required for Ψ sequencing, we performed demethylase-pseudouridine sequencing (DM-Ψ-seq) by using freshly isolated $lineage^-$ cells, which are hematopoietic stem and progenitor enriched cells, from 3-month-old and 29-month-old mice according to an elegant approach [14, 36] (Fig. 2A). The result revealed no difference of the bulk Ψ profile between young and aged HSPCs (Fig. 2B). We then wondered whether the percentage of Ψ on certain sites of the tRNAs exhibits difference between them. To address this question, we evaluated all of the Ψs on detectable tRNAs. The results revealed that the percentage of Ψ_{28}, Ψ_{32}, Ψ_{53} and Ψ_{54} of $tRNA^{His}$-GTG holds static between young and aged HSPCs (Fig. 2C and D), and the same to other detected tRNAs (Suppl. Fig. 2). Briefly, these results indicate that not only bulk Ψ profile but also the percentage of each Ψ on tRNAs exhibit no difference between young and aged HSPCs, which is consistent with the data that the toxicity of enforced PUS10 on HSPCs is independent on its enzymatic activity.

Aging-declined $CRL4^{DCAF1}$-mediated ubiquitination degradation signaling leads to the increase of PUS10

Given that PUS10 is increased in aged HSPCs and enforced PUS10 impairs the reconstitution capacity of HSPCs, we then wondered how PUS10 is increased with aging. Firstly, we examined the mRNA level of *Pus10* between young and aged HSPCs ($CD48^-$LSK) by RT-PCR, and the result revealed no difference of *Pus10* mRNA between them (Fig. 3A). To confirm this observation, we examined the mRNA

level of *Pus10* between young and aged HSCs by exploring published RNA-sequencing data, and the result revealed that the mRNA level of *Pus10* holds static between young and aged HSCs (Suppl. Fig. 3). Then, it is conceivable that the increase of PUS10 might be modulated via post-transcriptional modification manner. To test this hypothesis, we purified proteins interacting with PUS10 via affinity purification and we observed that the $CRL4^{DCAF1}$ complex, including DDB1, DCAF1 and CUL4B, interacts with PUS10 (Fig. 3B). $CRL4^{DCAF1}$ complex is E3 ubiquitin ligase targeting substrate for protein degradation [41]. To confirm this observation, we performed co-immunoprecipitation (Co-IP) assay by infecting HEK293T cells with S-protein, FLAG, and streptavidin-binding peptide (SFB)-tagged PUS10 together with Myc-tagged DDB1, DCAF1 or CUL4B respectively. Cell lysates were incubated with S-protein beads and probed with anti-Flag, anti-Myc antibodies. The result showed that PUS10 exhibits strong interaction with DDB1, DCAF1 and CUL4B (Fig. 3C).

Previous study has shown that $CRL4^{DCAF1}$ complex participates in ubiquitin dependent degradation [41], we then set out to determine whether $CRL4^{DCAF1}$ regulates PUS10 ubiquitination. Plasmids encoding SFB-tagged PUS10, Myc-tagged DDB1, DCAF1, CUL4B and HA-tagged wild type ubiquitin (Ub-WT), mutant ubiquitin (Ub-K48R) were co-transfected into HEK293T cells. 24 hours later, cell lysates were collected to detect the ubiquitination of PUS10. The result revealed that $CRL4^{DCAF1}$ vigorously promotes the ubiquitination of PUS10 in cells expressing wild type ubiquitin (Fig. 3D). Compared with wild type ubiquitin, the ubiquitination of PUS10 was completely abolished in cells expressing K48R ubiquitin, indicating that $CRL4^{DCAF1}$ promotes poly-ubiquitination of PUS10 via the formation of the K48 linkage.

Next, we set out to investigate whether the increase of PUS10 is due to the alteration of $CRL4^{DCAF1}$ in aged HSPCs. We first evaluated the expression of $CRL4^{DCAF1}$ complex in young and aged HSPCs. The result showed that the expression of DDB1 and CUL4B is decreased in aged HSPCs (The expression level of DCAF1 is too low to be detected) (Fig. 3E), which is negatively correlated with the alteration of PUS10

between young and aged HSPCs (Fig. 1A).

Given that the protein level of PUS10, but not mRNA level, is elevated in aged HSPCs (Fig. 1A and 3A), and that PUS10 is poly-ubiquitinated by $CRL4^{DCAF1}$ complex (Fig. 3D), and that DDB1 and CUL4B are decreased in aged HSPCs (Fig. 3E), we then wondered whether aging-declined $CRL4^{DCAF1}$ complex leads to the increase of PUS10. To test this hypothesis, we generated two efficient shRNAs against *Ddb*1 (Fig. 3F and H, Table S2), which is the key linker protein of $CRL4^{DCAF1}$ complex [41]. 32D cells were infected by sh*Ddb1* carring lentivirus for 72 hours, and GFP^+ cells were subjected to detect the protein level of PUS10 by western blot. The result showed that PUS10 is elevated upon the knockdown of *Ddb1* (Fig. 3F and G).

Taken together, these data suggest that aging-declined $CRL4^{DCAF1}$-mediated ubiquitination degradation signaling leads to the accumulation of PUS10.

Young *Pus10*$^{-/-}$ mice exhibit no influence on hematopoietic homeostasis and HSC function

The above results revealed the functional role of *Pus10* in modulating HSC aging, we then wondered whether targeted dysfunction of *Pus10* plays a role in regulating hematopoietic homeostasis and HSC function. To address this question, we generated *Pus10* knockout mice on C57BL/6N background by deleting the 2nd exon using CRISPR-Cas9 system (Fig. 4A, see details in Material and Method) and we achieved efficient deletion of PUS10 in LSK cells (Fig. 4B and C).

We then performed complete blood count assay for *Pus10*$^{-/-}$ and age-matched control mice. The result revealed no difference of white blood cell (WBC), lymphocyte (LYM), neutrophil (NEUT), red blood cell (RBC) and platelet (PLT) between *Pus10*$^{-/-}$ and WT mice (Fig. 4D). We then sought to investigate the lineage composition in peripheral blood (PB) and bone marrow (BM) of *Pus10*$^{-/-}$ mice, including T cells, B cells and myeloid cells (Suppl. Fig. 4A). The results revealed no difference of *Pus10*$^{-/-}$ mice compared to WT in PB (Fig. 4E) and BM (Fig. 4F).

We next analyzed hematopoietic stem and progenitor cells of *Pus10*$^{-/-}$ mice, including common myeloid progenitor (CMP), granulocyte-macrophage progenitor

(GMP), megakaryocyte-erythroid progenitor (MEP), common lymphoid progenitor (CLP), multipotent progenitor cell (MPP) and HSC (Suppl. Fig. 4B). The results revealed no significant difference of the above populations between *Pus10*$^{-/-}$ and WT mice (Fig. 4G-K).

To further investigate the reconstitution capacity of *Pus10*$^{-/-}$ HSCs, 20 freshly isolated *Pus10*$^{-/-}$ and WT HSCs were transplanted into lethally irradiated recipients together with 3×10^5 competitor cells (Fig. 5A). The chimera in PB of recipients was evaluated every four weeks until the 16th week (Suppl. Fig. 4C and D). The results showed that the reconstitution capacity of *Pus10*$^{-/-}$ HSCs is comparable with WT ones (Fig. 5B), while dysfunction of *Pus10* promotes the differentiation bias towards lymphoid lineage (34.31% vs 48.43%, Fig. 5C). Donor-derived HSCs of recipients revealed no significant difference between *Pus10*$^{-/-}$ and WT mice (Fig. 5D-F).

Aged *Pus10*$^{-/-}$ mice exhibit mild alteration of hematopoietic homeostasis and HSC function

We then investigated the phenomenon of aged *Pus10*$^{-/-}$ mice. We performed complete blood count assay for aged WT and *Pus10*$^{-/-}$ mice (26-month old). The result showed no significant difference of WBC, LYM, NEUT, RBC and platelet between aged WT and *Pus10*$^{-/-}$ mice (Fig. 6A). We then analyzed the frequency of T cells, B cells and myeloid cells in PB, BM, spleen and thymus of aged *Pus10*$^{-/-}$ and WT mice. The results revealed no significant difference between them in PB (Fig. 6B) and thymus (Fig. 6E). However, the percentage of T cells in BM (Fig. 6C) and the percentage of myeloid cells in spleen (Fig. 6D) of aged *Pus10*$^{-/-}$ mice are increased.

We next investigated hematopoietic stem and progenitor cells of aged *Pus10*$^{-/-}$ and WT mice. The results indicated no significant difference of the CMP, GMP, MEP, CLP and MPP, while the frequency of HSC is increased in aged *Pus10*$^{-/-}$ mice compared to WT (Fig. 6F-J).

To further explore the reconstitution capacity of aged *Pus10*$^{-/-}$ HSCs, 150 freshly isolated aged *Pus10*$^{-/-}$ and WT HSCs were transplanted into lethally irradiated recipients together with 3×10^5 competitor cells (Fig. 6K). The chimera in PB of

recipients was evaluated every four weeks until the 12th week. The results revealed that the reconstitution capacity of aged *Pus10*$^{-/-}$ HSCs is comparable with WT ones, while dysfunction of *Pus10* promotes the differentiation bias towards B lineage (Fig. 6L and M).

In brief, our study for the first time revealed that enforced PUS10 impairs the reconstitution capacity of HSPCs. Howere, the hematopoietic homeostasis and reconstitution capacity of young *Pus10*$^{-/-}$ mice is comparable with control mice, while aged *Pus10*$^{-/-}$ mice exhibit mild alteration of hematopoietic homeostasis and HSC function. In summary, these data suggest that aging-diminished CRL4^{DCAF1}-mediated ubiquitination degradation signaling leads to the accumulation of PUS10, which impairs HSPCs (Fig. 7).

DISCUSSION

Our study for the first time evaluated the role of PUS10 in HSC aging and function. This study will expand our understanding of RNA modification on HSC function regulation.

Post-transcriptional regulation in aged hematopoietic stem cells

An elegant study reported a proteomics resource from mass spectrometry of mouse young and aged HSCs, and identified a subset of genes with apparent post-transcriptional alteration during aging [40]. This indicates that transcriptomic levels may not reflect the functional change of aged HSCs. The alteration of protein level achieved either by RNA or protein modification in aged HSCs might play an essential role in promoting HSC aging. Our unpublished data confirmed this observation by identifying a group of RNA modification genes which modulating HSC aging. In addition, our study also identified CRL4^{DCAF1}-mediated ubiquitination participated in regulating HSC aging by degrading PUS10 and other important proteins (unpublished). Whether there are other proteins modified by ubiquitination lead to their changes during aging, thereby regulating HSC aging and other cell aging is a

question worthy of study. It is also intriguing to investigate the molecular mechanism why ubiquitin ligases are altered during aging.

Therefore, exploring the functional role of post-transcriptional modification (PTM) in aging might strengthen the understanding of aging on HSCs and clinical relevance.

RNA epigenetics vs HSC aging

In our study, we observed the Ψ profile is not changed in aged HSPCs and the aging-increased PUS10 promotes HSC aging, which is not achieved by its Ψ synthase activity. Up to date, there are more than 170 RNA modifications have been identified and some of them play essential role in various biological process and clinical diseases [42, 43]. Whether other RNA modification profiles are altered in aged HSCs and whether the corresponding enzymes are involved in regulating HSC aging is a question worthy of investigation. In this study, we performed Ψ profiling by using HSPCs, but not pure HSCs, due to the limitation of HSC number. Whether the Ψ profile of aged HSCs is identical as we observed in HSPCs is also a question worth investigating, which depends on the development of sequencing technology.

Supplemental Information

The supplemental information includes four figures and three tables.

Accession number

All sequencing raw data were deposited into the National Center for Biotechnology Information Gene Expression Omnibus. The accession code is GSE213422 with the enter token atstusiqpxmhvmj.

Reference

1. Dzierzak E, Bigas A. Blood Development: Hematopoietic Stem Cell Dependence and Independence. Cell Stem Cell. 2018;22(5):639-651.
2. Morrison SJ, Scadden DT. The bone marrow niche for haematopoietic stem cells. Nature. 2014;505(7483):327-334.
3. He H, Xu P, Zhang X, et al. Aging-induced IL27Ra signaling impairs hematopoietic stem cells. Blood. 2020;136(2):183-198.
4. Dykstra B, Olthof S, Schreuder J, Ritsema M, de Haan G. Clonal analysis reveals multiple functional defects of aged murine hematopoietic stem cells. J Exp Med. 2011;208(13):2691-2703.
5. Wang J, Sun Q, Morita Y, et al. A differentiation checkpoint limits hematopoietic stem cell self-renewal in response to DNA damage. Cell. 2012;148(5):1001-1014.
6. Mohrin M, Shin J, Liu Y, et al. Stem cell aging. A mitochondrial UPR-mediated metabolic checkpoint regulates hematopoietic stem cell aging. Science. 2015;347(6228):1374-1377.
7. Norddahl GL, Pronk CJ, Wahlestedt M, et al. Accumulating mitochondrial DNA mutations drive premature hematopoietic aging phenotypes distinct from physiological stem cell aging. Cell Stem Cell. 2011;8(5):499-510.
8. Sun D, Luo M, Jeong M, et al. Epigenomic profiling of young and aged HSCs reveals concerted changes during aging that reinforce self-renewal. Cell Stem Cell. 2014;14(5):673-688.
9. Boccaletto P, Stefaniak F, Ray A, et al. MODOMICS: a database of RNA modification pathways. 2021 update. Nucleic Acids Res. 2022;50(D1):D231-D235.
10. Cohn WE, Volkin E. Nucleoside-5′-Phosphates from Ribonucleic Acid. Nature. 1951;167(4247):483-484.
11. Charette M, Gray MW. Pseudouridine in RNA: what, where, how, and why. IUBMB Life. 2000;49(5):341-351.
12. Ge J, Yu YT. RNA pseudouridylation: new insights into an old modification. Trends Biochem Sci. 2013;38(4):210-218.
13. Spenkuch F, Motorin Y, Helm M. Pseudouridine: still mysterious, but never a fake (uridine)! RNA Biol. 2014;11(12):1540-1554.
14. Song J, Zhuang Y, Zhu C, et al. Differential roles of human PUS10 in miRNA processing and tRNA pseudouridylation. Nat Chem Biol. 2019;16(2):160-169.
15. Li X, Zhu P, Ma S, et al. Chemical pulldown reveals dynamic pseudouridylation of the mammalian transcriptome. Nat Chem Biol. 2015;11(8):592-597.
16. Guzzi N, Cieśla M, Ngoc PCT, et al. Pseudouridylation of tRNA-Derived Fragments Steers Translational Control in Stem Cells. Cell. 2018;173(5):1204-1216.
17. Levi O, Arava YS. Pseudouridine-mediated translation control of mRNA by methionine aminoacyl tRNA synthetase. Nucleic Acids Res. 2021;49(1):432-443.
18. Bernick DL, Dennis PP, Hochsmann M, Lowe TM. Discovery of Pyrobaculum small RNA families with atypical pseudouridine guide RNA features. RNA. 2012;18(3):402-411.
19. Ni J, Tien AL, Fournier MJ. Small nucleolar RNAs direct site-specific synthesis of pseudouridine in ribosomal RNA. Cell. 1997;89(4):565-573.
20. Keffer-Wilkes LC, Veerareddygari GR, Kothe U. RNA modification enzyme TruB is a tRNA chaperone. Proc Natl Acad Sci U S A. 2016;113(50):14306-14311.
21. Leppik M, Liiv A, Remme J. Random pseuoduridylation in vivo reveals critical region of

Escherichia coli 23S rRNA for ribosome assembly. Nucleic Acids Res. 2017;45(10):6098-6108.
22. Zhao X, Patton JR, Davis SL, Florence B, Ames SJ, Spanjaard RA. Regulation of nuclear receptor activity by a pseudouridine synthase through posttranscriptional modification of steroid receptor RNA activator. Mol Cell. 2004;15(4):549-558.
23. Anderson BR, Muramatsu H, Nallagatla SR. Incorporation of pseudouridine into mRNA enhances translation by diminishing PKR activation. Nucleic Acids Res. 2010; 38(17):5884-5892.
24. Kariko K, Muramatsu H, Welsh FA, et al. Incorporation of pseudouridine into mRNA yields superior nonimmunogenic vector with increased translational capacity and biological stability. Mol Ther. 2008;16(11):1833-1840.
25. Svitkin YV, Cheng YM, Chakraborty T, Presnyak V, John M, Sonenberg N. N1-methyl-pseudouridine in mRNA enhances translation through eIF2alpha-dependent and independent mechanisms by increasing ribosome density. Nucleic Acids Res. 2017;45(10):6023-6036.
26. Borchardt EK, Martinez NM, Gilbert WV. Regulation and Function of RNA Pseudouridylation in Human Cells. Annu Rev Genet. 2020;54:309-336.
27. Bykhovskaya Y, Casas K, Mengesha E, Inbal A, Fischel-Ghodsian N. Missense mutation in pseudouridine synthase 1 (PUS1) causes mitochondrial myopathy and sideroblastic anemia (MLASA). Am J Hum Genet. 2004;74(6):1303-1308.
28. Shaheen R, Han L, Faqeih E, et al. A homozygous truncating mutation in PUS3 expands the role of tRNA modification in normal cognition. Hum Genet. 2016;135(7):707-713.
29. Festen EA, Goyette P, Green T, et al. A meta-analysis of genome-wide association scans identifies IL18RAP, PTPN2, TAGAP, and PUS10 as shared risk loci for Crohn's disease and celiac disease. PLoS Genet. 2011;7(1):e1001283.
30. de Brouwer APM, Abou Jamra R, Körtel N, et al. Variants in PUS7 Cause Intellectual Disability with Speech Delay, Microcephaly, Short Stature, and Aggressive Behavior. Am J Hum Genet. 2018;103(6):1045-1052.
31. Darvish H, Azcona LJ, Alehabib E, et al. A novel PUS7 mutation causes intellectual disability with autistic and aggressive behaviors. Neurol Genet. 2019;5(5):e356.
32. Arroyo JD, Jourdain AA, Calvo SE, et al. A Genome-wide CRISPR Death Screen Identifies Genes Essential for Oxidative Phosphorylation. Cell Metab. 2016;24(6):875-885.
33. Guzzi N, Muthukumar S, Ciesla M, et al. Pseudouridine-modified tRNA fragments repress aberrant protein synthesis and predict leukaemic progression in myelodysplastic syndrome. Nat Cell Biol. 2022;24(3):299-306.
34. Bellodi C, McMahon M, Contreras A, et al. H/ACA small RNA dysfunctions in disease reveal key roles for noncoding RNA modifications in hematopoietic stem cell differentiation. Cell Rep. 2013;3(5):1493-1502.
35. Gu BW, Fan JM, Bessler M, Mason PJ. Accelerated hematopoietic stem cell aging in a mouse model of dyskeratosis congenita responds to antioxidant treatment. Aging Cell. 2011;10(2):338-348.
36. Cui Q, Yin K, Zhang X, et al. Targeting PUS7 suppresses tRNA pseudouridylation and glioblastoma tumorigenesis. Nat Cancer. 2021;2(9):932-949.
37. Termini CM, Pang A. Syndecan-2 enriches for hematopoietic stem cells and regulates stem cell repopulating capacity. Blood. 2022; 139(2):188-204.
38. Akinduro O, Weber TS, Ang H, et al. Proliferation dynamics of acute myeloid leukaemia and haematopoietic progenitors competing for bone marrow space. Nat Commun. 2018;9(1):519.
39. Tadokoro Y, Hoshii T, Yamazaki S, et al. Spred1 Safeguards Hematopoietic Homeostasis against

Diet-Induced Systemic Stress. Cell Stem Cell. 2018;22(5):713-725.

40. Zaro BW, Noh JJ, Mascetti VL, et al. Proteomic analysis of young and old mouse hematopoietic stem cells and their progenitors reveals post-transcriptional regulation in stem cells. eLife. 2020;9:e62210.

41. Jackson S, Xiong Y. CRL4s: the CUL4-RING E3 ubiquitin ligases. Trends Biochem Sci. 2009;34(11):562-570.

42. Shi H, Chai P, Jia R, Fan X. Novel insight into the regulatory roles of diverse RNA modifications: Re-defining the bridge between transcription and translation. Mol Cancer. 2020;19(1):78.

43. Delaunay S, Frye M. RNA modifications regulating cell fate in cancer. Nat Cell Biol. 2019;21(5):552-559.

FIGURE LEGENDS

Figure 1. Aging-activated PUS10 impairs the reconstitution capacity of HSPCs independently on its enzymatic activity.

(A) Representative western blot showing the expression of PUS10 in HSPCs between young (3 months) and aged (28 months) mice. (B) This histogram depicts the protein level of PUS10 in young and aged HSPCs from quantitative western blot data (n = 2). (C) The protein expression of PUS10 in the proteomics dataset of young and old HSCs. (D) Experimental design of the transplantation assay. (E) These line plots depict the changes in peripheral blood chimerism in recipients transplanted with Vector or PUS10-OE LSK (n = 7 mice per group). (F) This histogram displays the lineage distribution of myeloid, T and B cells among donor-derived cells in the peripheral blood of Vector and PUS10-OE recipients at the 12^{th} week (n = 7 mice per group). (G-H) Freshly isolated WT LSK cells were infected by PUS10-carrying lentivirus for 72 hours, and 50 GFP^+ HSPCs ($CD48^-$ LSK) were sorted into 96-well plate and cultured in SFEM medium for 7 days. Then, the clones from Vector or PUS10-OE HSPCs were photographed and the cell numbers of these clones were analyzed. (G) These images show the expansion of Vector or PUS10-OE HSPCs. (H) The scatter plots show the cell numbers of these clones. (I) The result of liquid chromatography-tandem mass spectrometry shows the Ψ/U ratio in WT and *Pus10*$^{-/-}$ LK cells with overexpression of wild-type PUS10 or $PUS10^{D342A}$. (J) These line plots display the changes in peripheral blood chimerism in recipients transplanted with Vector, PUS10-OE or $PUS10^{D342A}$-OE LSK (n = 7-8 mice per group). All data are shown as mean± SD; **P* < 0.05, ***P* < 0.01, ****P* < 0.001.

Figure 2. No difference of pseudouridine modification profile between young and aged HSPCs.

(A-D) $Lineage^-$ cells were isolated from young (3 months) and aged (29 months) mice. Small RNA (<200nt) was extracted and purified to perform DM–Ψ-seq. (A) Experimental design. (B) The scatter plot depicts pseudouridine levels in tRNA between young and aged HSPCs (n = 2). (C) Schematic of tRNA-His-GTG-2-1 shows pseudouridine sites Ψ28, Ψ32, Ψ53 and Ψ54. (D) Pseudouridine sites (red arrows) and

levels of tRNA-His-GTG-2-1 are identified in young and aged HSPCs. The x axis represents nucleotide position. The y axis represents pseudouridine levels.

Figure 3. Aging-declined CRL4^{DCAF1}-mediated ubiquitination degradation signaling leads to the increase of PUS10.

(A) This histogram depicts the mRNA expression of *Pus10* in young (2 months) and aged (31 months) HSPCs. (B) Affinity purification of PUS10 protein from HEK293T cells stably expressing Flag- tagged PUS10. Proteins identified by Mass Spectrometry are listed. The bait protein is marked in bold letters. (C) HEK293T cells were co-transfected with plasmids encoding SFB-tagged PUS10 and Myc-tagged DDB1, DCAF1, CUL4B followed by co-immunoprecipitation using anti-Flag, anti-Myc antibody. Representative western blot shows that PUS10 interacts with DDB1, DCAF1 and CUL4B. (D) HEK293T cells were co-transfected with plasmids encoding SFB-tagged PUS10, Myc-tagged DDB1, DCAF1, CUL4B and HA-tagged Ub-WT or Ub-K48R followed by co-immunoprecipitation using anti-HA, anti-Flag, anti-Myc antibody. Representative western blot shows that PUS10 is ubiquitinated by the CRL4^{DCAF1} complex. (E) Representative western blot shows the expressions of DDB1 and CUL4B in young (3 months) and aged (28 months) HSPCs. (F) 32D cells were infected by lentivirus carrying *Ddb1*-shRNA. 72 h later, GFP^{+} cells were sorted for western blot to validate the expression of PUS10 and DDB1. Representative western blot shows the expression of PUS10 and DDB1 in Vector and DDB1-KD 32D cells. (G) This histogram depicts the protein level of PUS10 in Vector and DDB1-KD 32D cells from quantitative western blot data (n = 2). (H) This histogram depicts the protein expression of DDB1 in Vector and DDB1-KD 32D cells from quantitative western blot data (n = 3).

Figure 4. Young *Pus10*$^{-/-}$ mice exhibit no influence on hematopoietic homeostasis.

(A) Schematic illustration of the *Pus10* knockout (*Pus10*$^{-/-}$) mice. (B) Representative western blot shows the expression of PUS10 in WT and *Pus10*$^{-/-}$ LSK cells. (C) This histogram depicts the protein expression of PUS10 in WT and *Pus10*$^{-/-}$ LSK cells from quantitative western blot data (n = 2). (D) The scatter plots show the cell numbers of white blood cell (WBC), lymphocyte (LYM), neutrophil (NEUT), red

blood cell (RBC) and platelet (PLT) between WT and *Pus10*$^{-/-}$ mice. (E-F) The scatter plots depict the frequency of B cells, T cells and myeloid cells in peripheral blood (E) and bone marrow (F) of WT and *Pus10*$^{-/-}$ mice. (G) The scatter plots show the cell numbers of bone marrow in WT and *Pus10*$^{-/-}$ femurs. (H-K) The scatter plots depict the cell numbers and frequency of CMPs (common myeloid progenitors), GMPs (granulocyte/macrophage progenitors), MEPs (megakaryocytic/erythroid progenitors), CLPs (common lymphoid progenitors), MPP (multipotent progenitor cell) and HSCs in WT and *Pus10*$^{-/-}$ femurs. All data are shown as mean± SD; **P* < 0.05, ***P* < 0.01, ****P* < 0.001.

Figure 5. Young *Pus10*$^{-/-}$ mice exhibit no influence on HSC function.

(A) Experimental design of the competitive transplantation strategy. (B) These line plots depict the changes in peripheral blood chimerism in recipients transplanted with WT or *Pus10*$^{-/-}$ HSCs (n = 5 mice per group). (C) This histogram displays the lineage distribution of myeloid, T and B cells among donor-derived cells in peripheral blood of the recipients at the 16th week (n = 5 mice per group). (D) The gating strategies for the frequency of the test donor-derived HSCs. (E-F) The scatter plots depict the cell numbers (E) and frequency (F) of donor-derived HSCs in recipients transplanted with WT or *Pus10*$^{-/-}$ HSCs (n = 5 mice per group). All data are shown as mean± SD; **P* < 0.05, ***P* < 0.01, ****P* < 0.001.

Figure 6. Aged *Pus10*$^{-/-}$ mice exhibit mild alteration of hematopoietic homeostasis and HSC function.

(A) The scatter plots show the cell numbers of white blood cell (WBC), lymphocyte (LYM), neutrophil (NEUT), red blood cell (RBC) and platelet (PLT) between aged WT and *Pus10*$^{-/-}$ mice. (B-E) The scatter plots depict the frequency of B cells, T cells and myeloid cells in peripheral blood (B), bone marrow (C), spleen (D) and thymus (E) of aged WT and *Pus10*$^{-/-}$ mice. (F) The scatter plots show the cell numbers of bone marrow in WT and *Pus10*$^{-/-}$ femurs. (G-J) The scatter plots indicate the cell numbers and frequency of CMPs (common myeloid progenitors), GMPs (granulocyte/macrophage progenitors), MEPs (megakaryocytic/erythroid progenitors), CLPs (common lymphoid progenitors), MPP (multipotent progenitor cell) and HSCs

in WT and *Pus10*$^{-/-}$ femurs. (K) Experimental design of the transplantation assay. (L) These line plots depict the changes in peripheral blood chimerism in recipients transplanted with aged WT or *Pus10*$^{-/-}$ HSCs (n = 8-10 mice per group). (M) This histogram displays the lineage distribution of myeloid, T and B cells among donor-derived cells in peripheral blood of the recipients at the 12th week (n = 8-10 mice per group). All data are shown as mean± SD; *P < 0.05, **P < 0.01, ***P < 0.001.

Figure 7. Aging-enforced PUS10 mediated by the decrease of ubiquitination degradation impairs HSPCs.

The proposed model diagram illustrates the accumulation of PUS10 mediated by the decrease of ubiquitination degradation during aging impairs HSPCs.

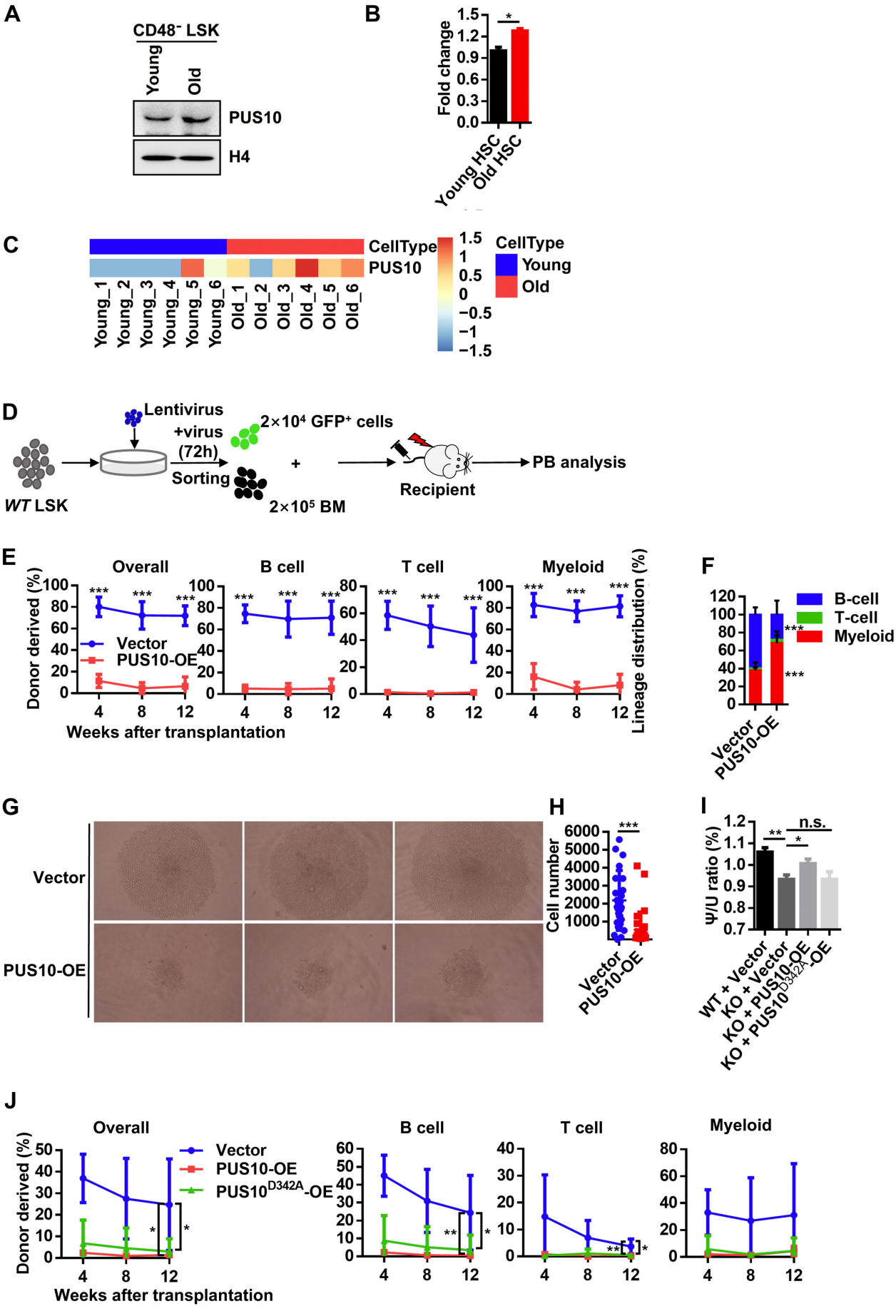
A
CD48⁻ LSK
Young
Old
PUS10
H4
B
Fold change
Young HSC
Old HSC
C
CellType
PUS10
Young_1
Young_2
Young_3
Young_4
Young_5
Young_6
Old_1
Old_2
Old_3
Old_4
Old_5
Old_6
CellType
Young
Old
D
Lentivirus
+virus
(72h)
Sorting
2×10⁴ GFP⁺ cells
2×10⁵ BM
WT LSK
Recipient
PB analysis
E
Overall
B cell
T cell
Myeloid
Donor derived (%)
Vector
PUS10-OE
Weeks after transplantation
Lineage distribution (%)
F
B-cell
T-cell
Myeloid
Vector
PUS10-OE
G
Vector
PUS10-OE
H
Cell number
Vector
PUS10-OE
I
Ψ/U ratio (%)
n.s.
WT + Vector
KO + Vector
KO + PUS10-OE
KO + PUS10D342A-OE
J
Overall
B cell
T cell
Myeloid
Donor derived (%)
Vector
PUS10-OE
PUS10D342A-OE
Weeks after transplantation

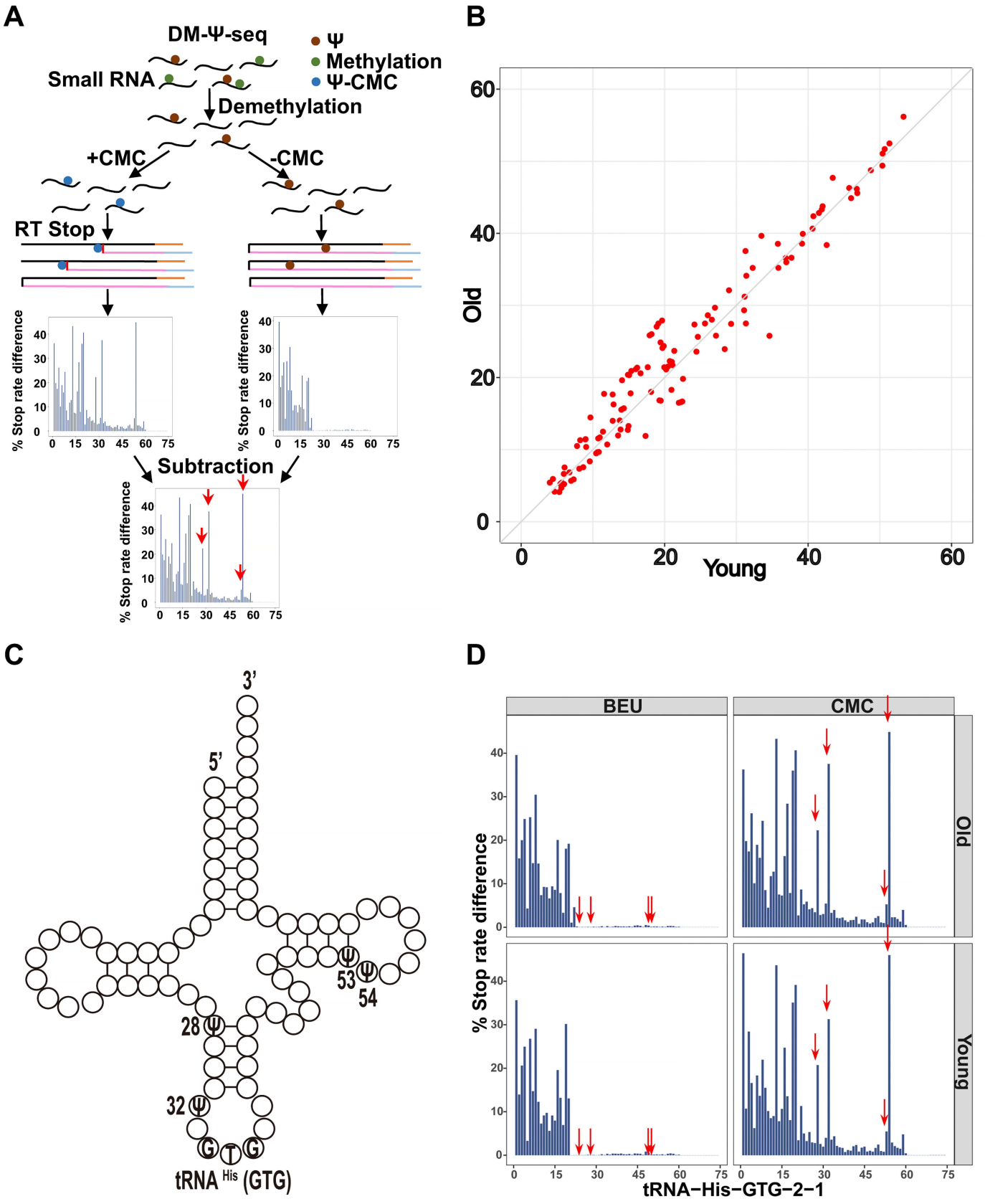
A
DM-Ψ-seq
Small RNA
Ψ
Methylation
Ψ-CMC
Demethylation
+CMC
-CMC
RT Stop
% Stop rate difference
Subtraction
B
Old
Young
C
3'
5'
28Ψ
32Ψ
53Ψ
54Ψ
GTG
tRNA His (GTG)
D
BEU
CMC
Old
Young
% Stop rate difference
tRNA-His-GTG-2-1

A

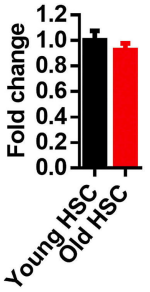

B

Protein	Unique Peptides
PUS10	3825
DDB1	3
DCAF1	2
CUL4B	1

C

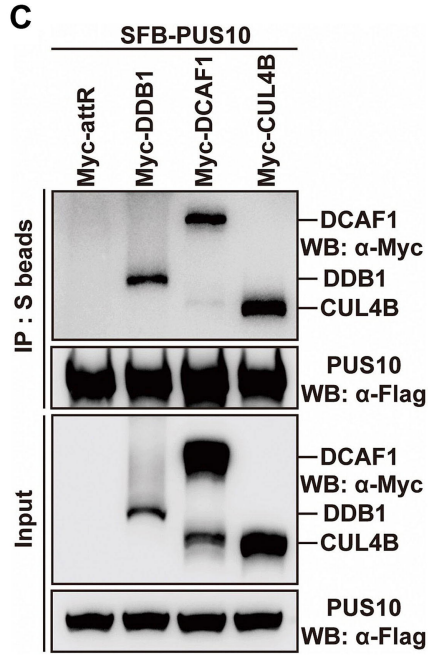

D

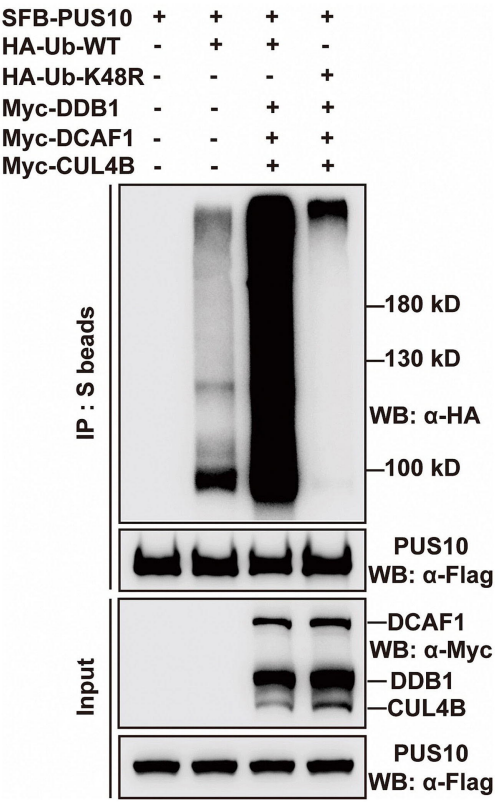

E

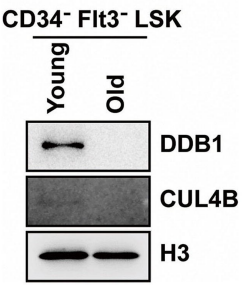

F

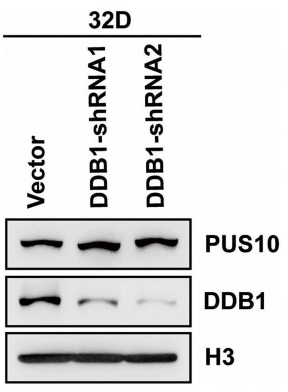

G

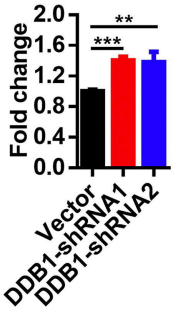

H

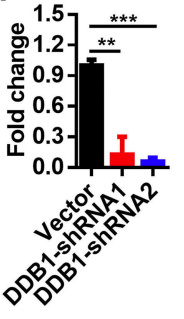

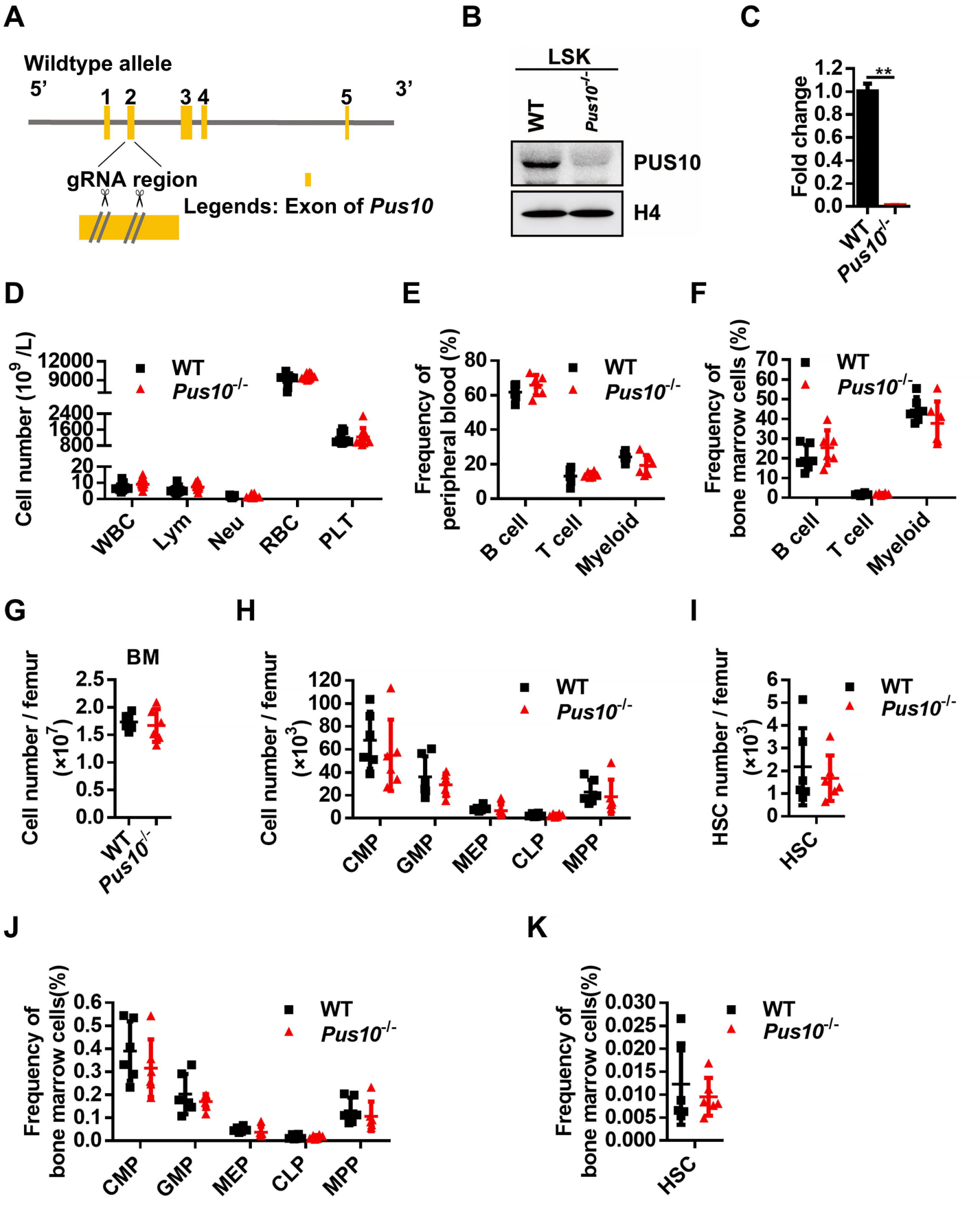
A
Wildtype allele
5'
1 2 3 4 5
3'
gRNA region
Legends: Exon of Pus10
B
LSK
WT
Pus10-/-
PUS10
H4
C
Fold change
1.2
1.0
0.8
0.6
0.4
0.2
0.0
**
WT
Pus10-/-
D
Cell number (10^9 /L)
12000
9000
2400
1600
800
20
10
0
WT
Pus10-/-
WBC
Lym
Neu
RBC
PLT
E
Frequency of peripheral blood (%)
80
60
40
20
0
WT
Pus10-/-
B cell
T cell
Myeloid
F
Frequency of bone marrow cells (%)
70
60
50
40
30
20
10
0
WT
Pus10-/-
B cell
T cell
Myeloid
G
BM
Cell number / femur (×10^7)
2.5
2.0
1.5
1.0
0.5
0.0
WT
Pus10-/-
H
Cell number / femur (×10^3)
120
100
80
60
40
20
0
WT
Pus10-/-
CMP
GMP
MEP
CLP
MPP
I
HSC number / femur (×10^3)
6
5
4
3
2
1
0
WT
Pus10-/-
HSC
J
Frequency of bone marrow cells(%)
0.6
0.5
0.4
0.3
0.2
0.1
0.0
WT
Pus10-/-
CMP
GMP
MEP
CLP
MPP
K
Frequency of bone marrow cells(%)
0.030
0.025
0.020
0.015
0.010
0.005
0.000
WT
Pus10-/-
HSC

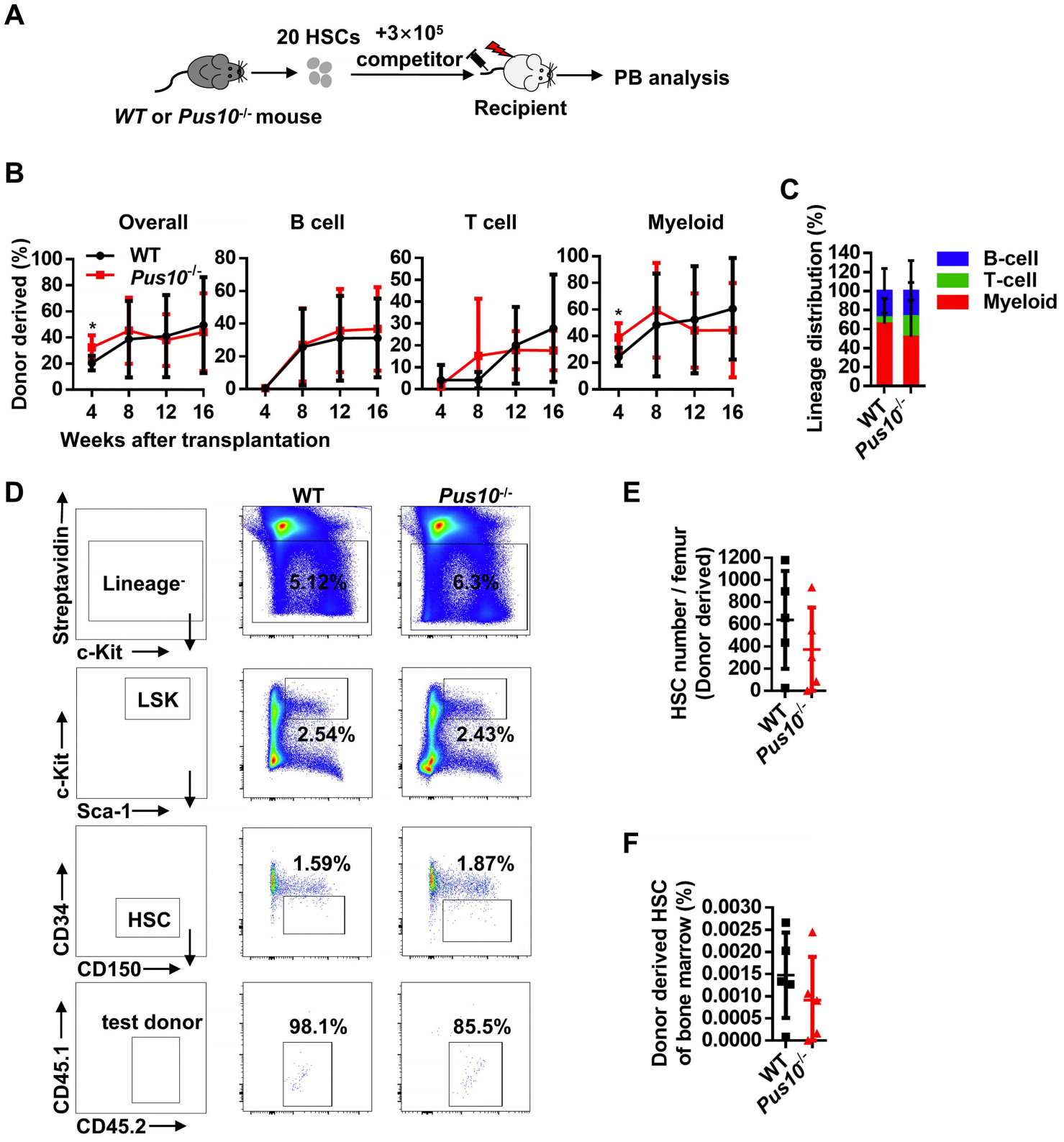
A
20 HSCs
+3×10^5
competitor
PB analysis
WT or Pus10-/- mouse
Recipient
B
Overall
B cell
T cell
Myeloid
WT
Pus10-/-
Donor derived (%)
Weeks after transplantation
C
Lineage distribution (%)
B-cell
T-cell
Myeloid
WT
Pus10-/-
D
WT
Pus10-/-
Streptavidin
Lineage-
c-Kit
5.12%
6.3%
LSK
c-Kit
Sca-1
2.54%
2.43%
HSC
CD34
CD150
1.59%
1.87%
test donor
CD45.1
CD45.2
98.1%
85.5%
E
HSC number / femur
(Donor derived)
WT
Pus10-/-
F
Donor derived HSC
of bone marrow (%)
WT
Pus10-/-

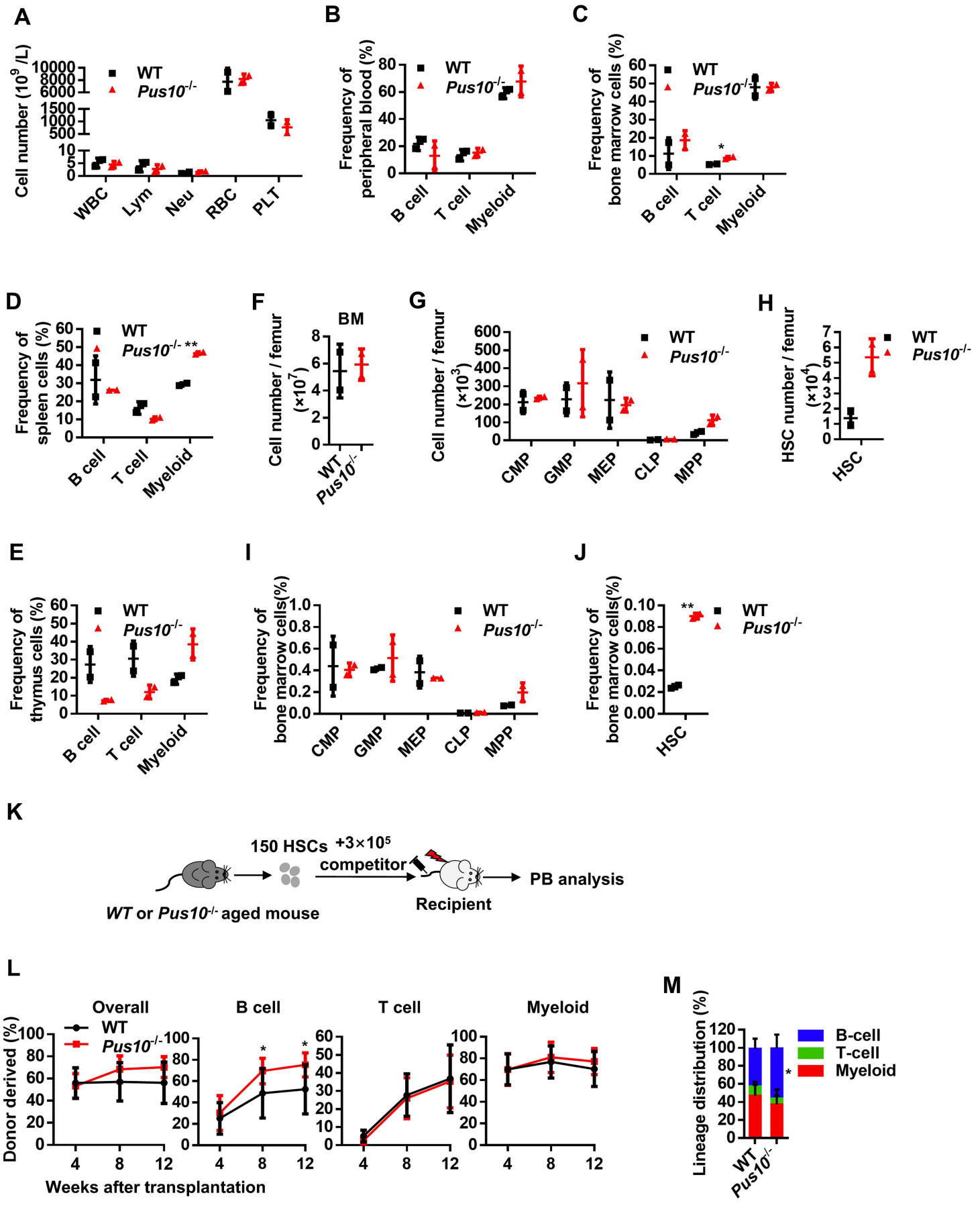
A
Cell number (10^9 /L)
WT
Pus10-/-
WBC
Lym
Neu
RBC
PLT
B
Frequency of peripheral blood (%)
B cell
T cell
Myeloid
C
Frequency of bone marrow cells (%)
*
D
Frequency of spleen cells (%)
Pus10-/- **
F
BM
Cell number / femur (×10^7)
G
Cell number / femur (×10^3)
CMP
GMP
MEP
CLP
MPP
H
HSC number / femur (×10^4)
HSC
E
Frequency of thymus cells (%)
I
Frequency of bone marrow cells(%)
J
**
K
150 HSCs
+3×10^5
competitor
PB analysis
Recipient
WT or Pus10-/- aged mouse
L
Overall
B cell
T cell
Myeloid
Donor derived (%)
Weeks after transplantation
M
Lineage distribution (%)
B-cell
T-cell
Myeloid

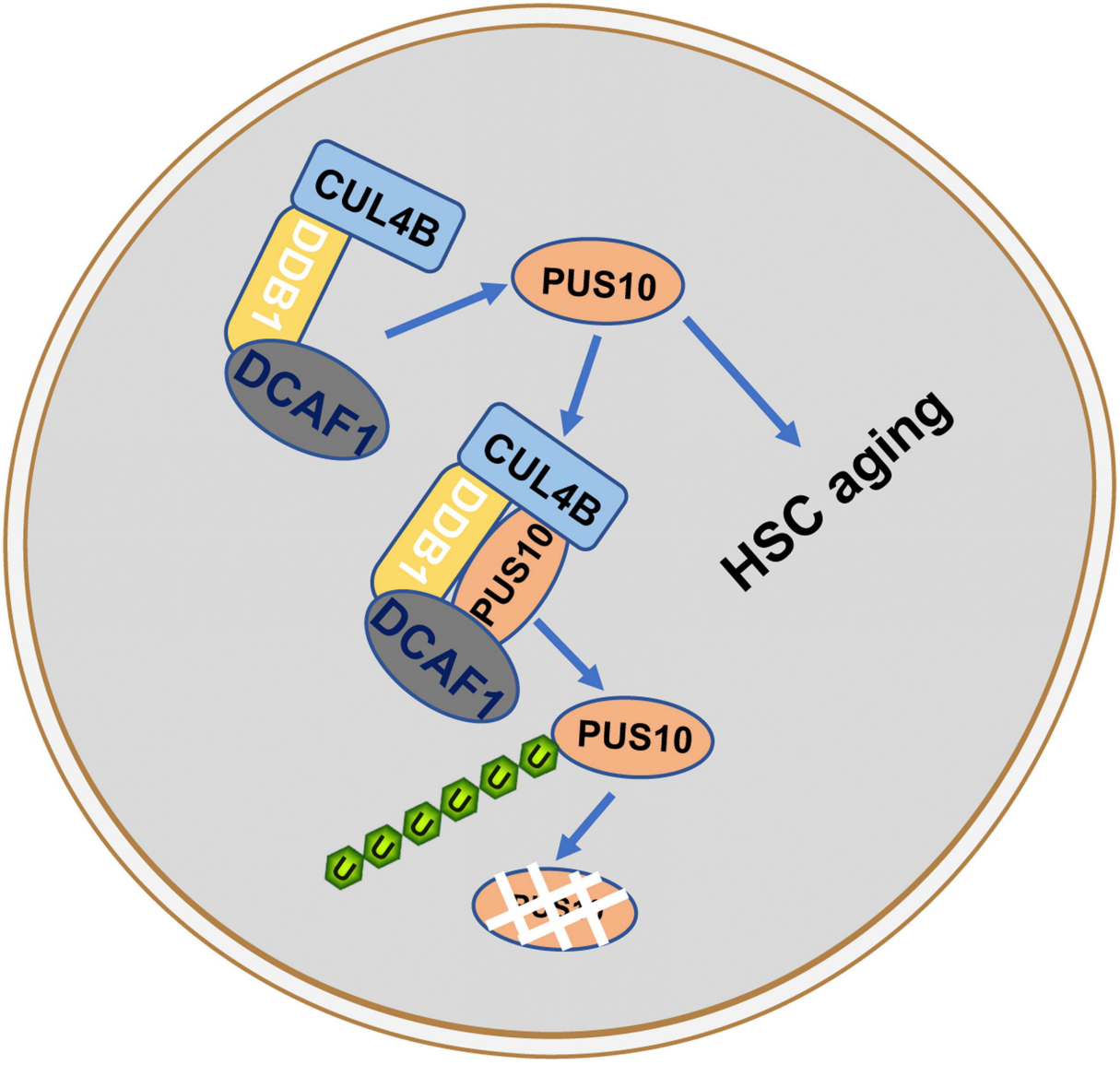
CUL4B
DDB1
DCAF1
PUS10
CUL4B
DDB1
PUS10
DCAF1
PUS10
HSC aging

Supplemental Methods

Lentivirus Production and Transduction

The mouse cDNA (*Pus10* or *Pus10*^{D342A}) was cloned into the pRRL-PPT-SF-newMCS-IRES2-EGFP vector. The *Ddb1*-shRNA sequence was cloned into SF-LV-miRE-EGFP vector. Lentivirus was produced in HEK293T cells and concentrated by ultracentrifugation at 25000 rpm for 2.5 h. For lentiviral transduction, LSK (cKit$^+$ Sca1$^+$ Lineage$^-$) cells were sorted and cultured in 96-well plate (~1 × 10^5 cells per well) with 100ul SFEM medium (Stem Cell Technology, 09650) containing 20 ng/ml mSCF, 20 ng/ml mTPO and 1 % penicillin/streptomycin. Lentivirus was added to LSK cells. 72 h later, 2x10^4 GFP$^+$ cells were sorted and injected into lethally irradiated recipients.

Flow Cytometric Analysis and Cell Sorting

Bone marrow cells were harvested from femurs, tibias and pelvis. Viable cells were counted by Vi-CELL XR Cell Viability Analyzer (Beckman Coulter). Bone marrow cells were applied for hematopoietic cell and lineage cell analysis. Hematopoietic cells (antibodies containing CD117, Sca1, Lineage cocktail, CD34, CD150, CD127, CD135 and CD16/32) and lineage cells (antibodies containing CD3, B220 and CD11b) were stained with fluorochrome labeled antibodies and identified by BD LSRFortessa flow cytometer. For Chimerism analysis, red cells in peripheral blood were lysed by ACK buffer (150 mM NH_4Cl, 10 mM $KHCO_3$, 0.1 mM Na_2EDTA, pH7.2-7.4). Lineage cells stained with fluorochrome labeled antibodies (antibodies containing CD3, B220, CD11b, CD45.1 and CD45.2) and analyzed by flow cytometer. Data were analyzed using FlowJo software. For hematopoietic stem and progenitor cells sorting, cKit$^+$ cells were enriched, then stained with antibodies. LSK cells, HSPCs and HSCs were sorted by BD Influx. The antibodies were listed in Table S1.

Transplantations and peripheral blood analysis

2x10^4 GFP$^+$ LSK cells (CD45.2) and 2x10^5 competitor cells (CD45.1) were injected into lethally irradiated (10 Gy) recipient mice (CD45.2). 20 or 150 HSCs (CD45.2) and 3x10^5 competitor cells (CD45.1) were injected into lethally irradiated (10 Gy) recipient mice (CD45.1/2). Peripheral blood of recipients was collected to analyze donor-derived

chimerism (myeloid, B, and T cells) every 4 weeks until the 12^{th} or 16^{th} week.

HSPCs in vitro cultures

50 HSPCs ($CD48^-$ LSK) were sorted into 96-well plate by BD Influx and cultured in SFEM medium containing 20 ng/ml mSCF, 20 ng/ml mTPO and 1 % penicillin/streptomycin for 7 days. Then, the clones were photographed and the cell numbers of these clones were analyzed by BD LSRFortessa flow cytometer and FlowJo software.

Quantification of Ψ by liquid chromatography-tandem mass spectrometry

RNA was extracted and purified using miRNeasy Mini Kit (Qiagen). The RNA was digested into single nucleosides by Nucleoside Digestion Mix (NEB). These nucleosides were detected by a label-free quantitation method. Finally, the Ψ/U ratio was analyzed.

Real-time PCR

Total RNA was isolated using TRIzol reagent (Invitrogen) according to the manufacturer's instruction. Total RNA was reverse transcribed by PrimeScript RT reagent Kit (Takara), followed by RT-PCR using PowerUp™ SYBR™ Green mix (Applied Biosystems) with indicated primers on a QuantStudio-3 Real-time PCR System (Applied Biosystems). The primers were listed in Table S3.

Western Blot

Freshly isolated HSPCs or 32D cells were lysed in sodium dodecyl sulfate (SDS) loading buffer, sonicated for 5 cycles using Bioruptor (Diagenode) and denatured by boiling at 100℃ for 5 min. Samples were resolved on 10% SDS-PAGE, and the separated proteins were transferred onto a PVDF membrane. Membranes were blocked with 5% skimmed milk in Tris-buffered saline with Tween-20 (TBST) buffer for 1 h at room temperature and then probed with primary antibodies overnight at 4 °C.

32D cells were harvested and lysed with NETN buffer (20 mM Tris-HCl, pH 8.0, 100 mM NaCl, 1 mM EDTA, 0.5% Nonidet P-40, containing protease and phosphatase inhibitors cocktail) on ice for 30 minutes followed by centrifugation at 12000 rpm for 5 min. The supernatant was mixed with 2× protein loading buffer and denatured by boiling at 100 ℃ for 5 min. Samples were loaded onto 10% SDS-PAGE gel, and the

separated proteins were transferred onto a PVDF membrane. Membranes were blocked with 5% skimmed milk in Tris-buffered saline with Tween-20 (TBST) buffer for 1 h at room temperature and then probed with primary antibodies overnight at 4 °C.

Affinity Purification and Mass Spectrometry

HEK293T cells stably expressing Flag-tagged PUS10 were lysed in NETN buffer on ice for 30 min followed by centrifugation at 12000 rpm for 5 min. The supernatant was transferred to a fresh microcentrifuge tube and incubated with anti-Flag beads at 4 ℃ for 4 hr. Beads were washed with NTEN buffer 3 times and boiled in 30 μL 2 x protein loading buffer. Samples were loaded onto 10% SDS-PAGE gel and analyzed by mass spectrometry.

Co-Immunoprecipitations

Plasmids encoding SFB-tagged PUS10 or Myc-tagged DDB1, DCAF1, CUL4B were co-transfected into HEK293T cells. 24 hr later, the transfected HEK293T cells were harvested and lysed with NETN buffer on ice for 30 minutes followed by centrifugation at 12000 rpm for 5 min. The supernatant was transferred to a fresh microcentrifuge tube and incubated with 20 μL S-protein beads at 4 ℃ for 2 hr. Beads were washed with NETN buffer 3 times, mixed with 2× protein loading buffer and denatured by boiling. Samples were loaded onto 10% SDS-PAGE gel, and the separated proteins were transferred onto a PVDF membrane. Membranes were blocked and then probed with anti-Flag, anti-Myc antibodies.

Ubiquitination assay

Plasmids encoding SFB-tagged PUS10, Myc-tagged DDB1, DCAF1, CUL4B and HA-tagged Ub-WT, Ub-K48R were co-transfected into HEK293T cells. 24 hr later, the transfected HEK293T cells were harvested and lysed with 100 μL denaturing TS buffer (50 mM Tris-HCl, pH 7.5, 1% SDS, 5 mM N-ethymaleimide). The lysates were boiled at 100 ℃ for 10 min and sonicated for 5 cycles using Bioruptor (Diagenode). The lysates were diluted with 900 μL TNN buffer (0.5% Nonidet P-40, 50 mM Tris-HCl, pH 7.5, 250 mM NaCl, 5 mM N-ethymaleimide) followed by centrifugation at 12000 rpm for 10 min. The supernatant was transferred to a fresh microcentrifuge tube and incubated with 20 μL S-protein beads at 4 ℃ for 2 hr. Beads were washed with NETN

buffer 3 times, mixed with 2× protein loading buffer and denatured by boiling. Samples were loaded onto 10% SDS-PAGE gel, and the separated proteins were transferred onto a PVDF membrane. Membranes were blocked and then probed with anti-HA, anti-Flag, anti-Myc antibodies.

Blood Cell Counts

Peripheral blood was collected from mice and analyzed using an Auto Hematology Analyzer BC-5000 (MINDRAY).

Statistical analysis

Data are shown as mean ± SD. Student's t test (Two-tailed unpaired) was used for comparisons between the groups using GraphPad Prism 6.0 software.

Supporting Tables

Table S1 Key resources table

REAGENT or RESOURCE	SOURCE	IDENTIFIER
Antibodies		
Ter-119-Biotin	BioLegend	TER-119
Gr-1-Biotin	BioLegend	RB6-8C5
CD11b-Biotin	BioLegend	M1/70
CD11b-PerCP-Cy5.5	BioLegend	M1/70
CD3e-Biotin	BioLegend	145-2C11
CD3e-APC	BioLegend	145-2C11
CD4-Biotin	BioLegend	GK1.5
CD8a-Biotin	BioLegend	53-6.7
B220-Biotin	BioLegend	RA3-6B2
B220-V500	BioLegend	RA3-6B2
B220-Pacific Blue	BioLegend	RA3-6B2
Sca-1-PE-Cy7	BD Biosciences	D7
CD117-APC	BD Biosciences	2B8
CD150-PE	BioLegend	TC15-12F12.2
CD48-FITC	BioLegend	HM48-1
CD48-PerCP-Cy5.5	BioLegend	HM48-1
CD34-AlexaFlour700	eBioscience	RAM34
CD34-FITC	eBioscience	RAM34
CD135-CF594	BD Biosciences	A2F10.1
CD135-PE	BD Biosciences	A2F10.1
CD16/32-FITC	BD Biosciences	2.4G2
CD127-BV421	BD Biosciences	A7R34
CD45.1-FITC	BD Biosciences	A20
CD45.1-PE	BD Biosciences	A20
CD45.1-AlexaFluor700	BD Biosciences	A20
CD45.2-FITC	BD Biosciences	104
CD45.2-PE	BD Biosciences	104
CD45.2- PerCP-Cy5.5	BD Biosciences	104
Streptavidin-APC-Cy7	BioLegend	
PUS10	Abcam	ab185078
Myc	Biodragon	B1002
Flag	Cell Signaling Technology	2368S
HA	Cell Signaling Technology	3724S
CUL4B	Abclonal	A12696
DDB1	Abcam	Ab109027
H3	Cell Signaling Technology	4499
H4	Cell Signaling Technology	13919
GAPDH	Biodragon	B1034

Actin	Cell Signaling Technology	4970
Rabbit anti-mouse IgG (HRP conjugate)	Cell Signaling Technology	58802
Mouse anti-rabbit IgG (HRP conjugate)	Cell Signaling Technology	93702
Chemicals, Peptides, and Recombinant Proteins		
SCF	Peprotech	#250-03
TPO	Peprotech	#315-14
DMSO	Sigma-Aldrich	D2650
Fetal Bovine Serum	GEMINI	900-108
DMEM	Gibco	C11995500BT
StemSpan serum-free medium	Stem Cell Technologies	09650
DAPI	Sigma–Aldrich	D8417
Penicillin–streptomycin	Gibco	15140122
D-Hanks	Solarbio	H1045
Hepes	Solarbio	H1095
PBS	Solarbio	P1022
TRIzol	Invitrogen	15596018
Critical Commercial Assays		
PrimeScript RT Reagent Kit	Takara	RR047A
PowerUp SYBR Green mix	Applied Biosystems	A25780
miRNeasy Mini Kit	Qiagen	217004
RNeasy MinElute Cleanup Kit	Qiagen	74204
RNase-Free DNase Set	Sangon Biotech	B618253
Deposited Data		
Small RNA DM–Ψ-seq data		
Experimental Models: Cell Lines		
HEK293T	ATCC	
Experimental Models: Organisms/Strains		
Mouse: *Pus10*$^{-/-}$ mice	Mo Li Laboratory	N/A
Mouse: C57BL/6 (CD45.2)	Jackson Laboratory	N/A
Mouse: C57BL/6-SJL (CD45.1)	Jackson Laboratory	N/A
Oligonucleotides		
Primers for mouse genotyping and qRT-PCR, see Table S3	This paper	N/A
Recombinant DNA		
pRRL-PPT-SF-newMCS-IRES2-EGFP (Vector)	This paper	N/A
pRRL-*mPus10*	This paper	N/A
SF-LV-miRE-EGFP (Vector)	This paper	N/A
miRE-*Ddb1*-shRNA1	This paper	N/A
miRE-*Ddb1*-shRNA2	This paper	N/A

SFB-*hPus10*	This paper	N/A
HA-Ub-WT	Yuancai Liu Lab	N/A
HA-Ub-K48R	Yuancai Liu Lab	N/A
Myc-hDdb1	Yeguang Chen Lab	N/A
Myc-hDcaf1	This paper	N/A
Myc-hCul4b	Qiang Ding Lab	N/A
Software and Algorithms		
FlowJo Software	Becton, Dickinson and Company	N/A
GraphPad Prism 6	GraphPad Software	N/A
Adobe Illustrator CS6	Adobe	N/A
Adobe Photoshop CS5	Adobe	N/A

Table S2 The sequence of *Pus10*-gRNA and *Ddb1*-shRNA

Gene	Sequence	Application
Pus10-gRNA A1	TAGGTGCTTGTTCTCCTCAGTCAG	*Pus10*$^{-/-}$ mice
Pus10-gRNA A2	AAACCTGACTGAGGAGAACAAGCA	*Pus10*$^{-/-}$ mice
Pus10-gRNA B1	TAGGGCACAGCTGTTGTTCAGTTC	*Pus10*$^{-/-}$ mice
Pus10-gRNA B2	AAACGAACTGAACAACAGCTGTGC	*Pus10*$^{-/-}$ mice
Ddb1-shRNA1	TAGCATGAGAACTCTTGTCTGG	Knockdown DDB1
Ddb1-shRNA2	TAGGTCTCTAGTGAACTGGTTT	Knockdown DDB1

Table S3 Primers for genotyping and RT-PCR

Gene	Forward	Reverse	Application
Pus10	CAGCACGTAGCTGTAGAATACTG	GTTTGTAAGGTGCGGGAAGA	Genotyping
Pus10	TATTACGAAGGTGTGCCAAAAGG	GGACTACATCATTTCTTCCCAGG	RT-PCR
Actin	GTGACGTTGACATCCGTAAAGA	GCCGGACTCATCGTACTCC	RT-qPCR

Supplemental Figure Legends

Supplemental figure 1. Aging-activated PUS10 impairs the reconstitution capacity of HSPCs independently on its enzymatic activity.

(A) Representative western blot shows the efficient overexpression of PUS10 in lineage$^-$ cells with lentivirus carrying cDNA of *Pus10*. (B) This histogram depicts the protein level of PUS10 in lineage$^-$ cells with lentivirus carrying cDNA of *Pus10* from quantitative western blot data (n = 5). (C) The gating strategies for the frequency of indicated donor-derived GFP$^+$ cells. (D) The gating strategies for quantifying lineage distribution of the test donor-derived GFP$^+$ cells (B, T, myeloid cells).

Supplemental figure 2. No difference of pseudouridine modification profile between young and aged HSPCs.

Schematic of identified pseudouridine sites are marked in individual tRNA. Pseudouridine sites (red arrows) and levels of individual tRNA are identified in young and aged HSPCs. The x axis represents nucleotide position. The y axis represents pseudouridine levels.

Supplemental figure 3. Aging-declined CRL4^{DCAF1}-mediated ubiquitination degradation signaling leads to the increase of PUS10.

The expression of *Pus10* between young and old HSCs in the GSE27686, GSE39553, GSE4332 and GSE6503 datasets.

Supplemental figure 4. Young *Pus10*$^{-/-}$ mice exhibit no influence on hematopoietic homeostasis and HSC function.

(A) The gating strategies for the frequency of B, T, myeloid cells in PB and BM of WT and *Pus10*$^{-/-}$ mice. (B) The gating strategies for quantifying the progenitors and HSCs in WT and *Pus10*$^{-/-}$ mice. (C) The gating strategies for the frequency of indicated donor-derived CD45.2$^+$ cells. (D) The gating strategies for quantifying lineage distribution of the test donor-derived CD45.2$^+$ cells (B, T, myeloid cells).

Supplemental figure 1

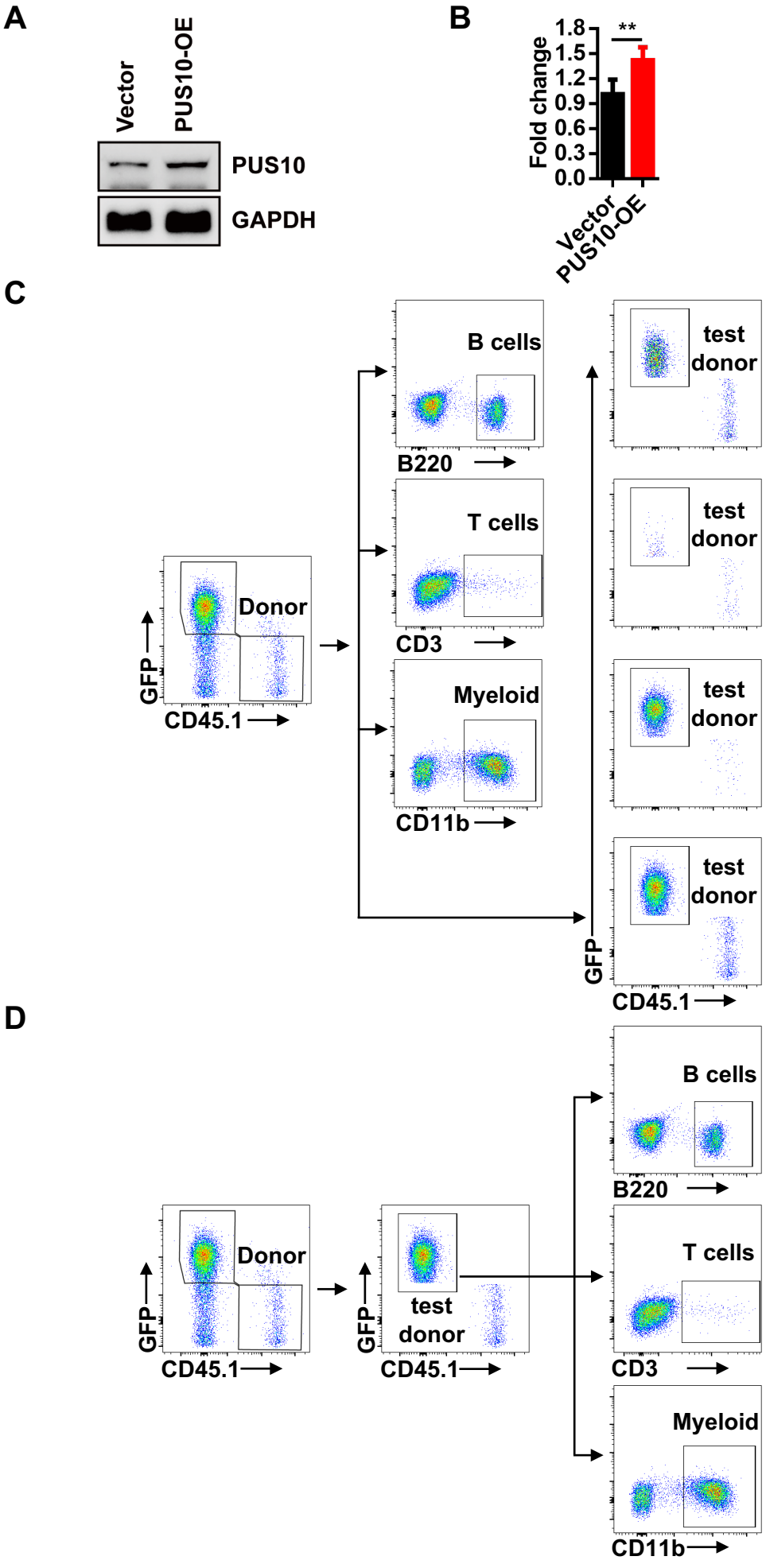

Supplemental figure 2

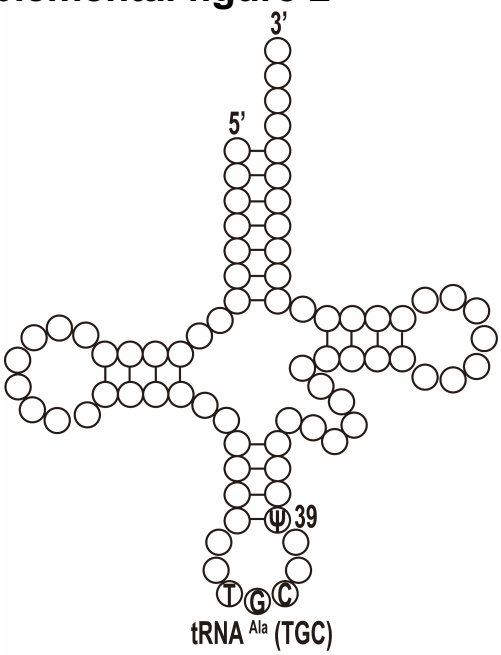

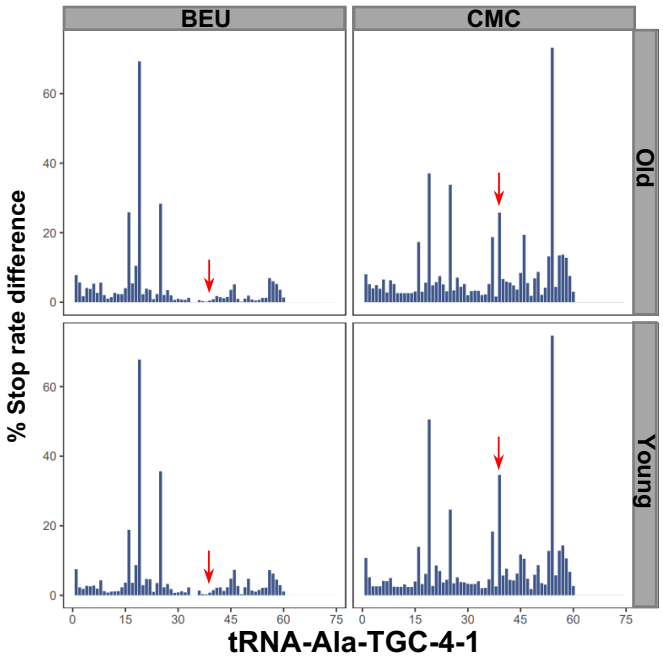

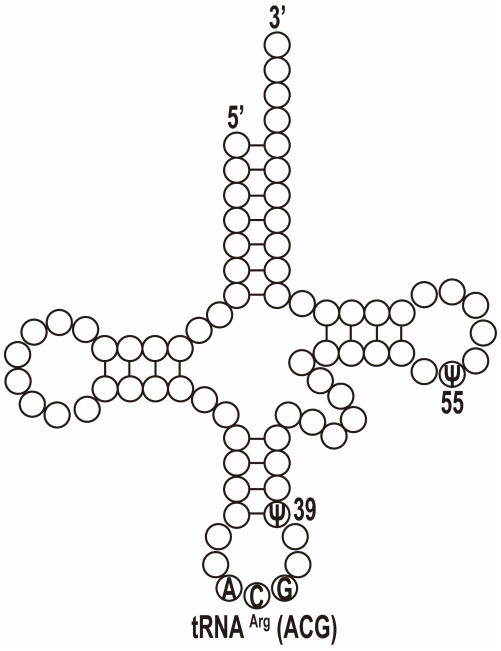

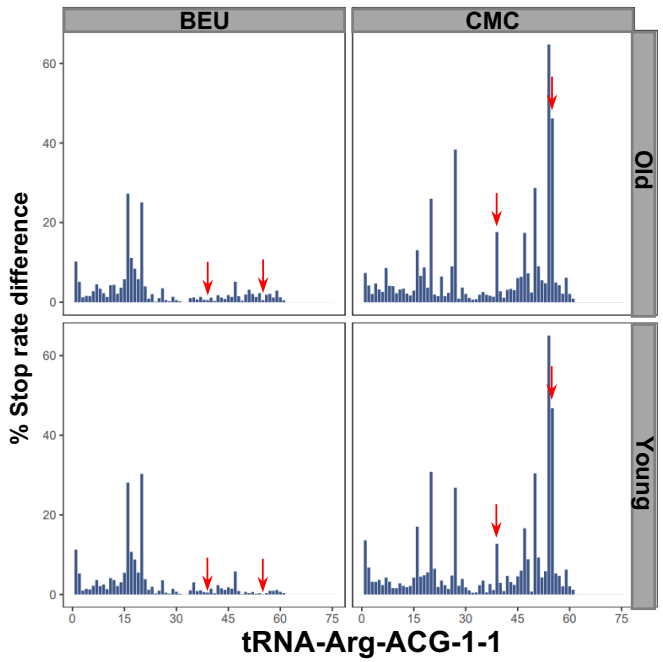

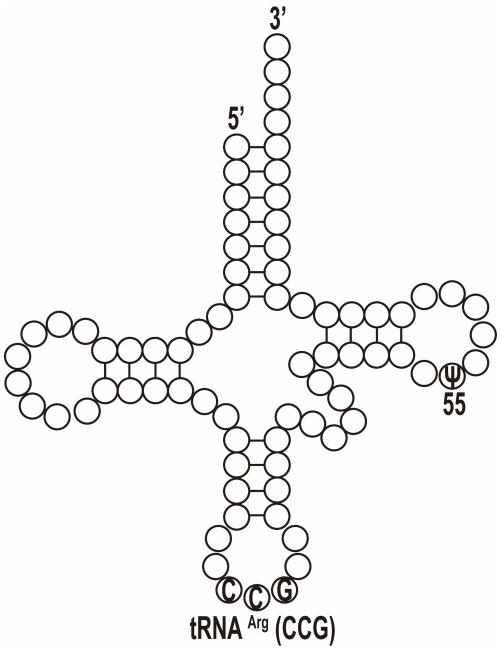

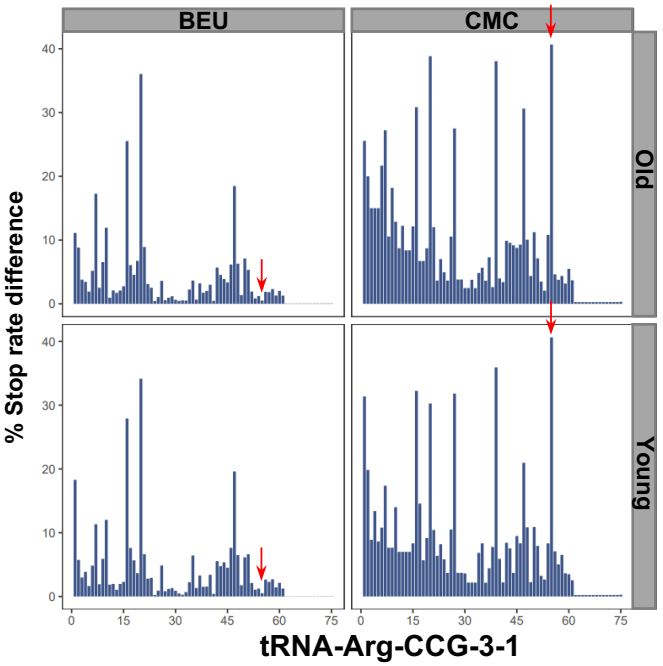

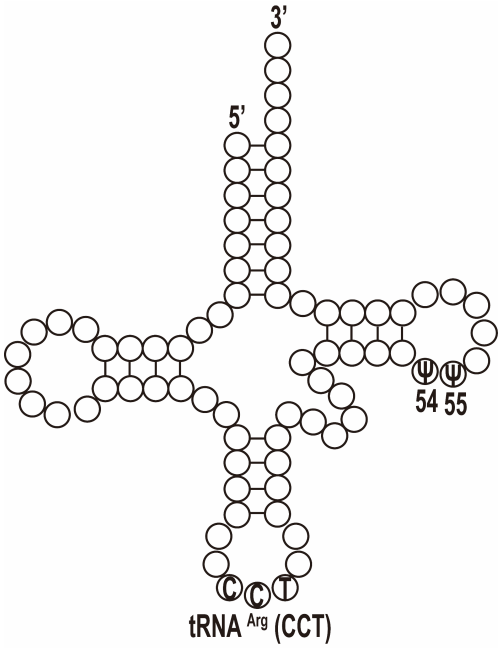
3'
5'
Ψ Ψ
54 55
C C T
tRNA Arg (CCT)

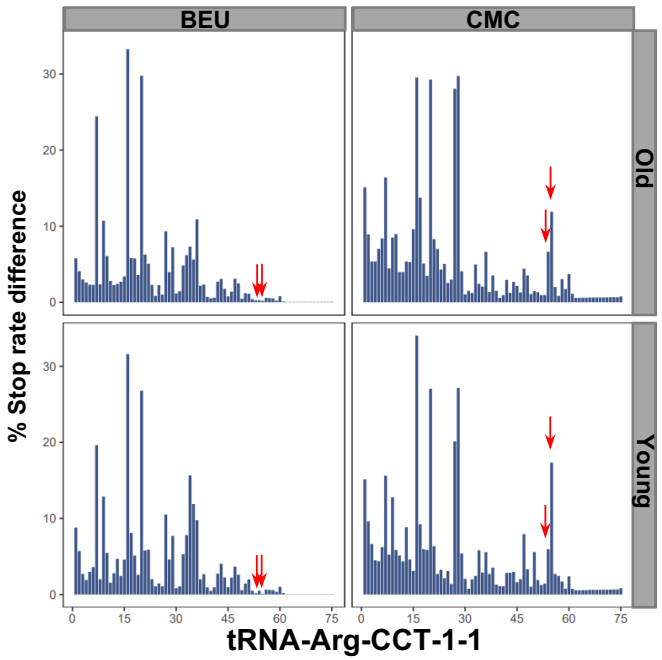
BEU
CMC
Old
Young
% Stop rate difference
0
10
20
30
0 15 30 45 60 75
tRNA-Arg-CCT-1-1

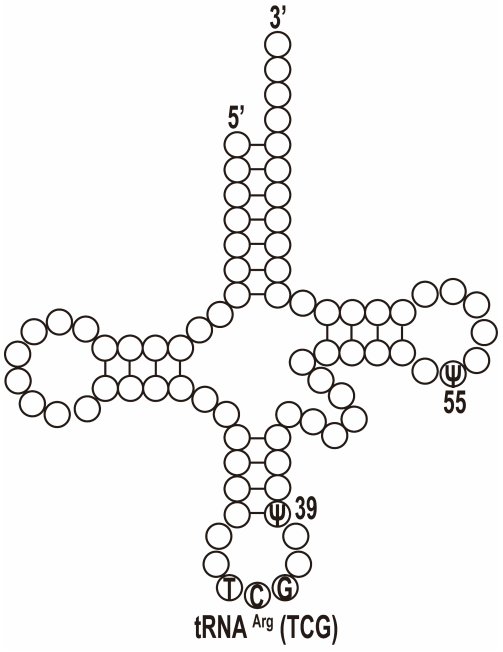
3'
5'
Ψ
55
Ψ 39
T C G
tRNA Arg (TCG)

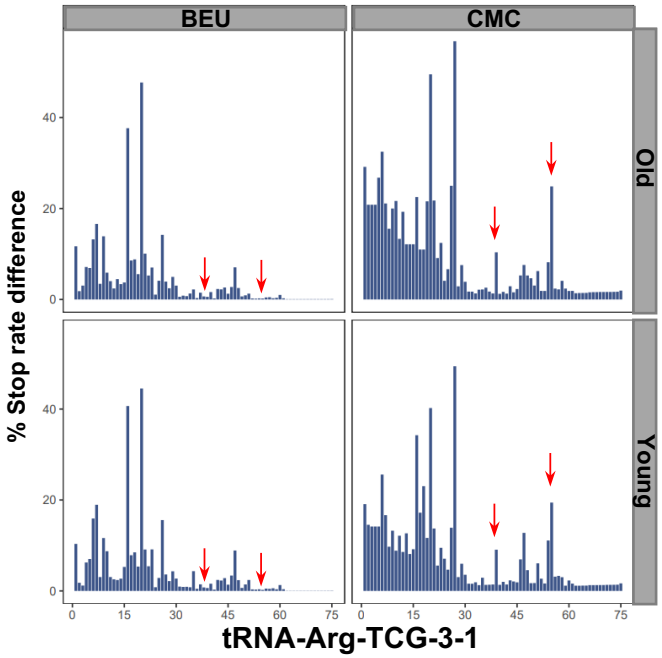
BEU
CMC
Old
Young
% Stop rate difference
0
20
40
0 15 30 45 60 75
tRNA-Arg-TCG-3-1

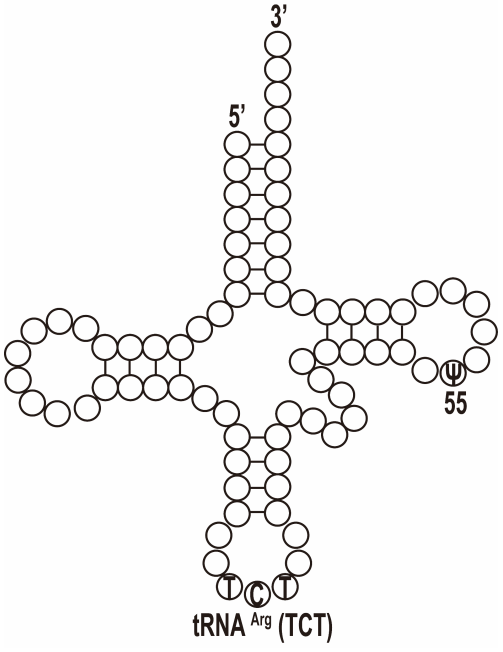
3'
5'
Ψ
55
T C T
tRNA Arg (TCT)

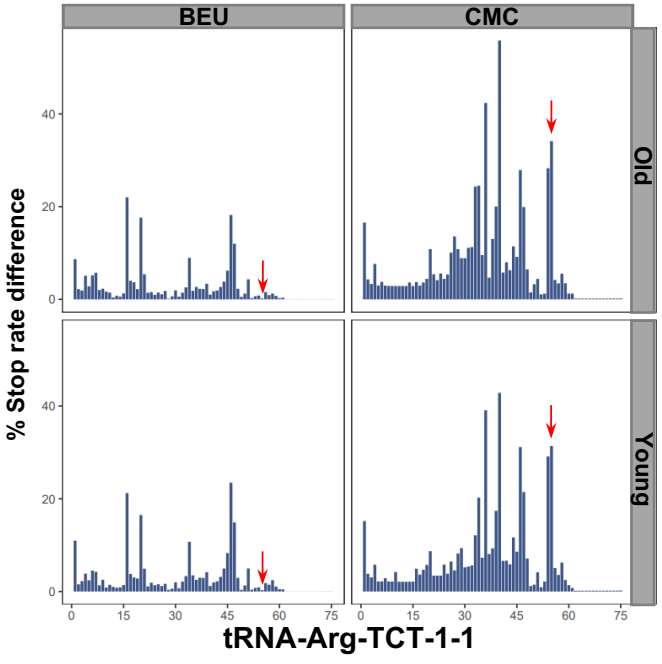
BEU
CMC
Old
Young
% Stop rate difference
0
20
40
0 15 30 45 60 75
tRNA-Arg-TCT-1-1

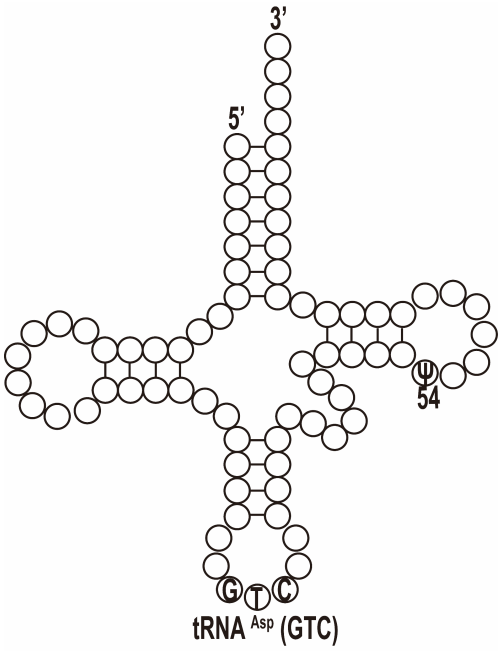
3'
5'
Ψ
54
G T C
tRNA Asp (GTC)

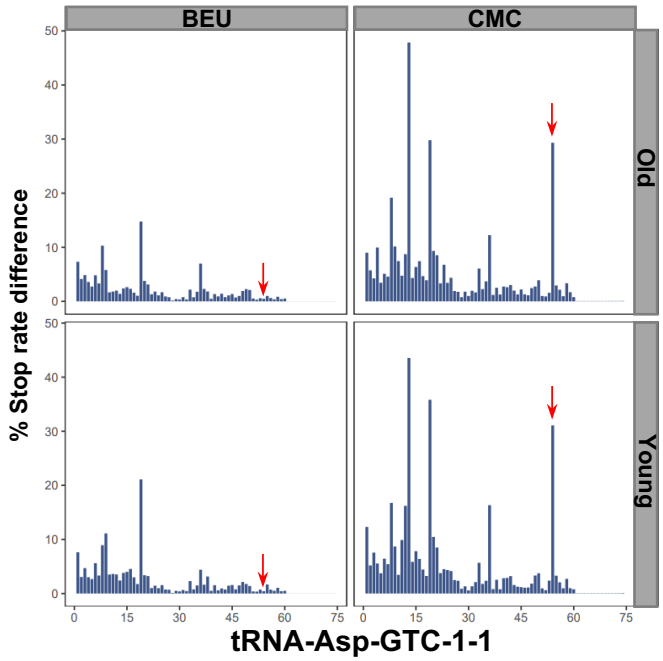
BEU
CMC
Old
Young
% Stop rate difference
tRNA-Asp-GTC-1-1

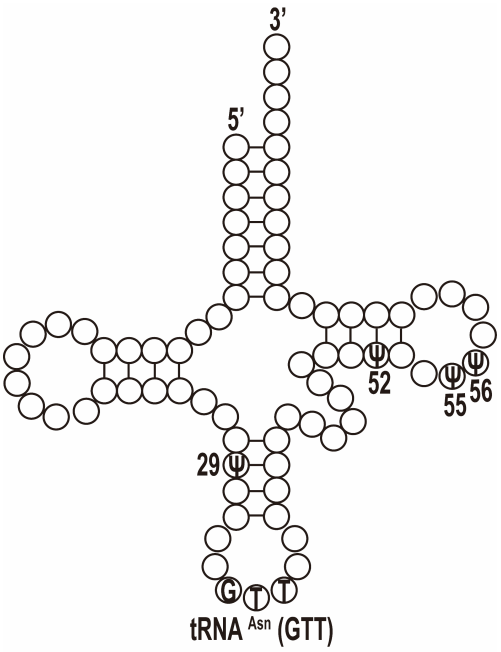
3'
5'
Ψ
52
55
56
29
G T T
tRNA Asn (GTT)

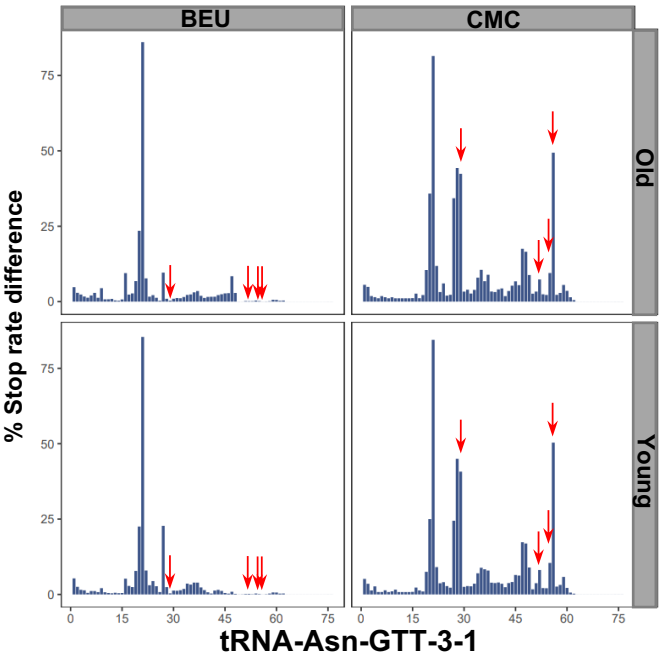
BEU
CMC
Old
Young
% Stop rate difference
tRNA-Asn-GTT-3-1

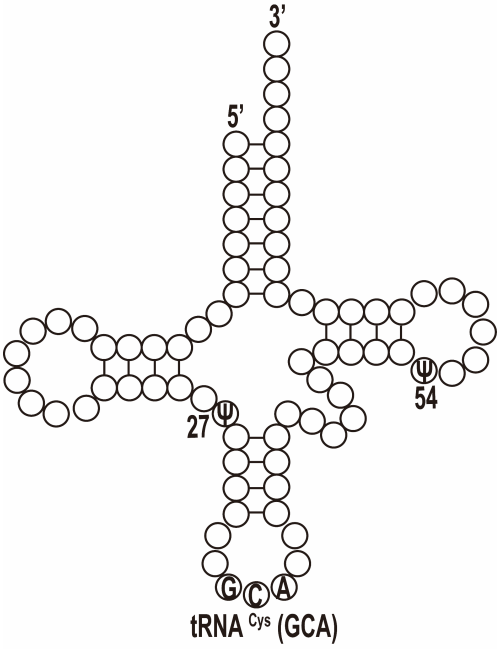
3'
5'
Ψ
54
27
G C A
tRNA Cys (GCA)

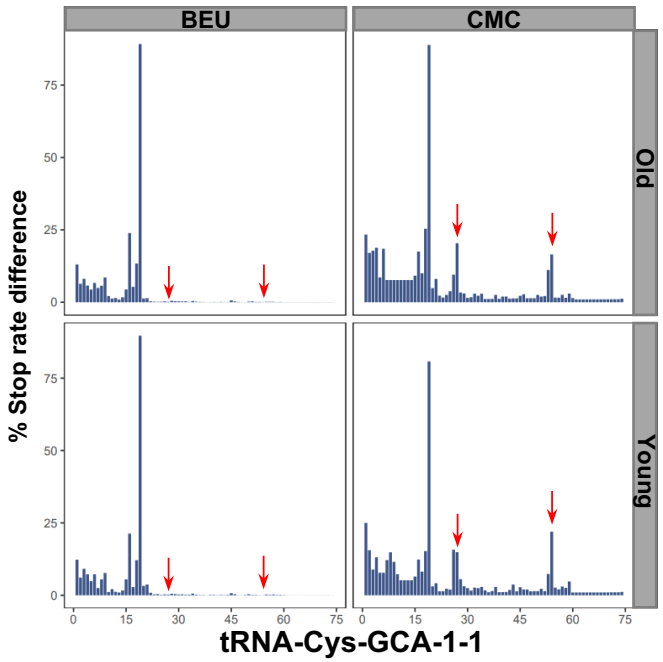
BEU
CMC
Old
Young
% Stop rate difference
tRNA-Cys-GCA-1-1

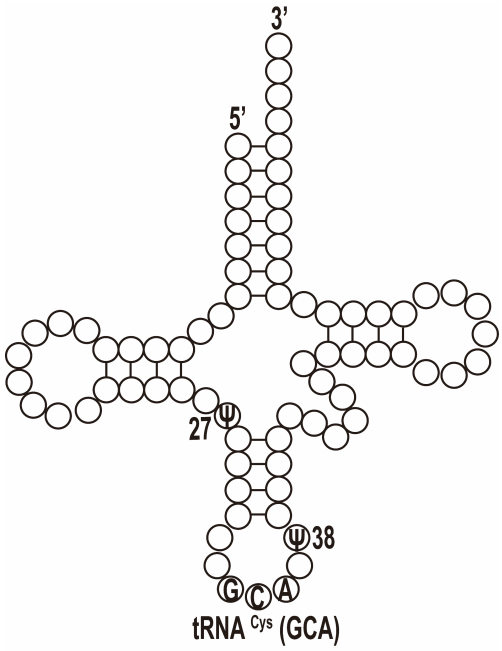
3'
5'
27Ψ
Ψ38
G C A
tRNA Cys (GCA)

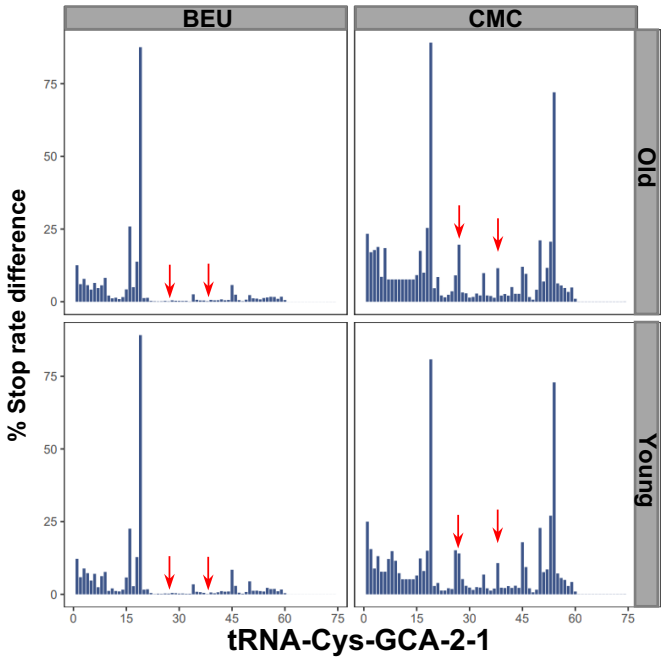
BEU
CMC
Old
Young
% Stop rate difference
tRNA-Cys-GCA-2-1

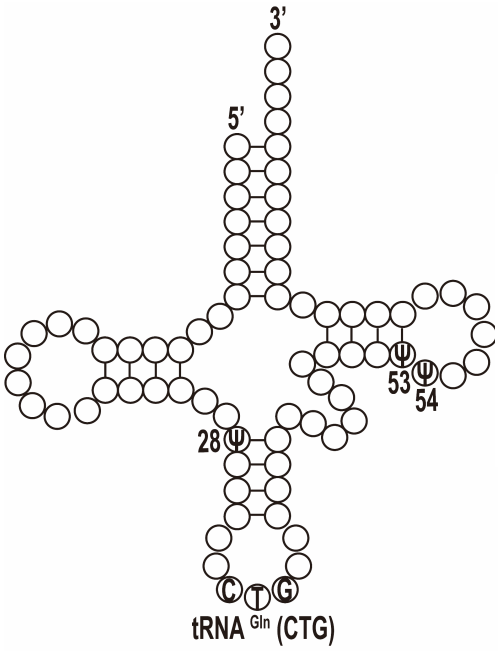
3'
5'
28Ψ
53Ψ
54
C T G
tRNA Gln (CTG)

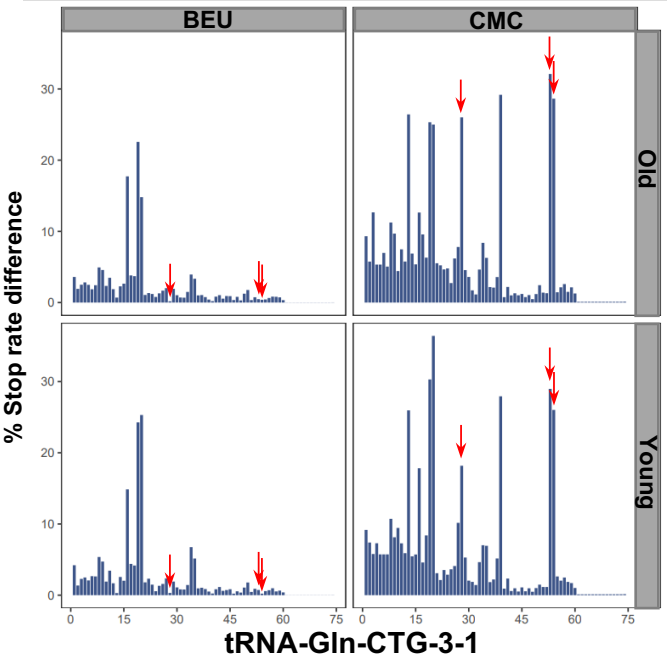
BEU
CMC
Old
Young
% Stop rate difference
tRNA-Gln-CTG-3-1

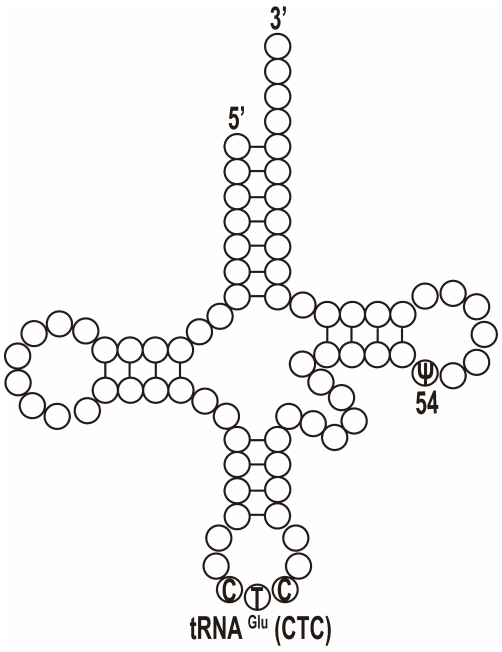
3'
5'
54
C T C
tRNA Glu (CTC)

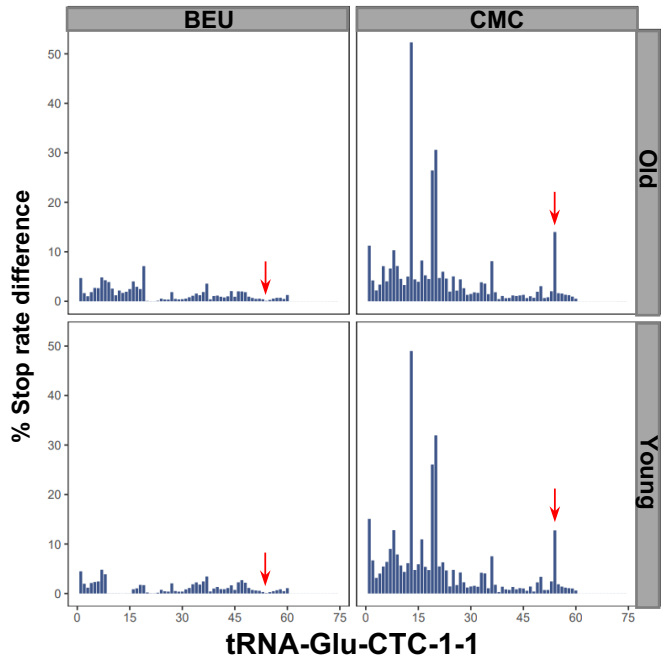
BEU
CMC
Old
Young
% Stop rate difference
tRNA-Glu-CTC-1-1

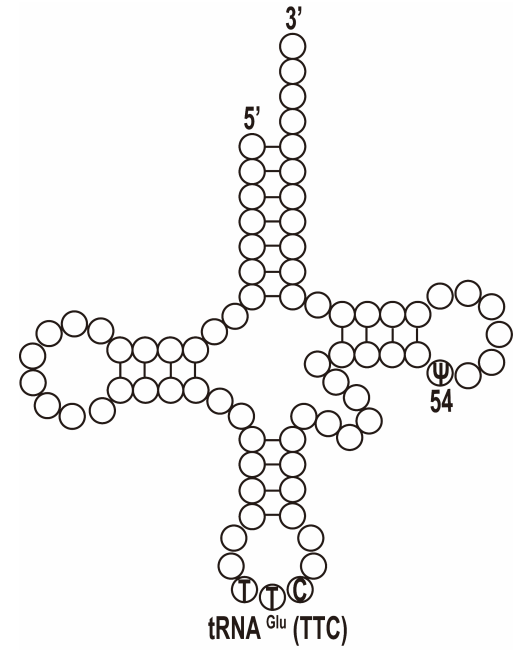
3'
5'
Ψ
54
T
T
C
tRNA Glu (TTC)

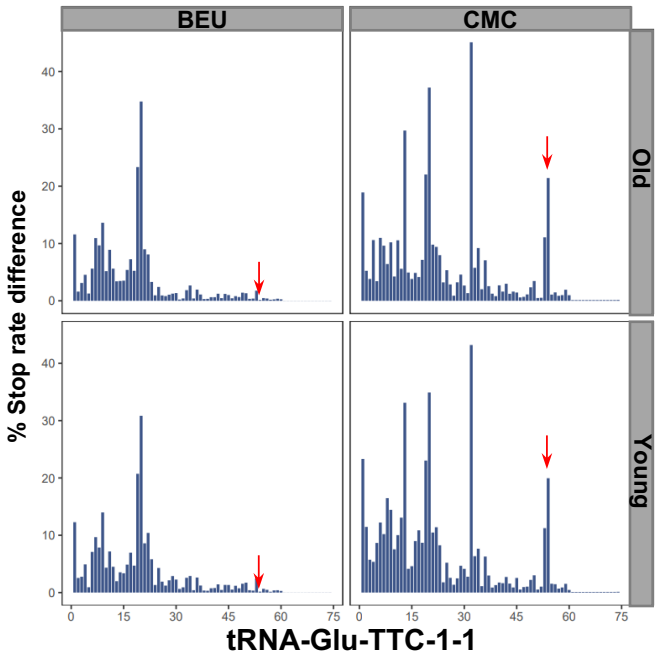
BEU
CMC
Old
Young
% Stop rate difference
0
10
20
30
40
0
15
30
45
60
75
tRNA-Glu-TTC-1-1

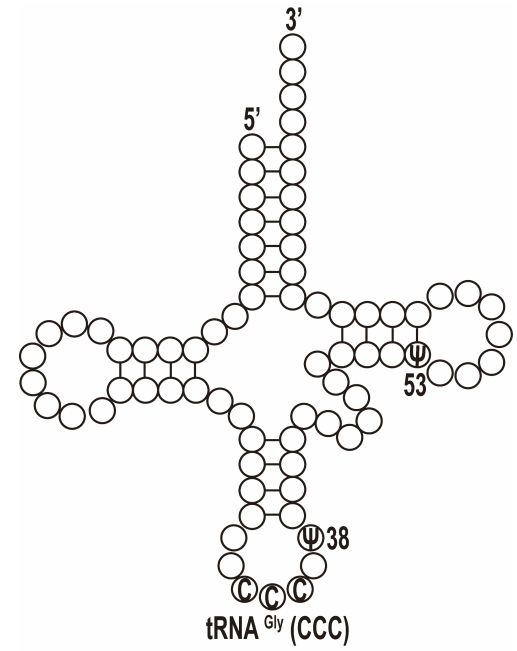
3'
5'
Ψ
53
Ψ
38
C
C
C
tRNA Gly (CCC)

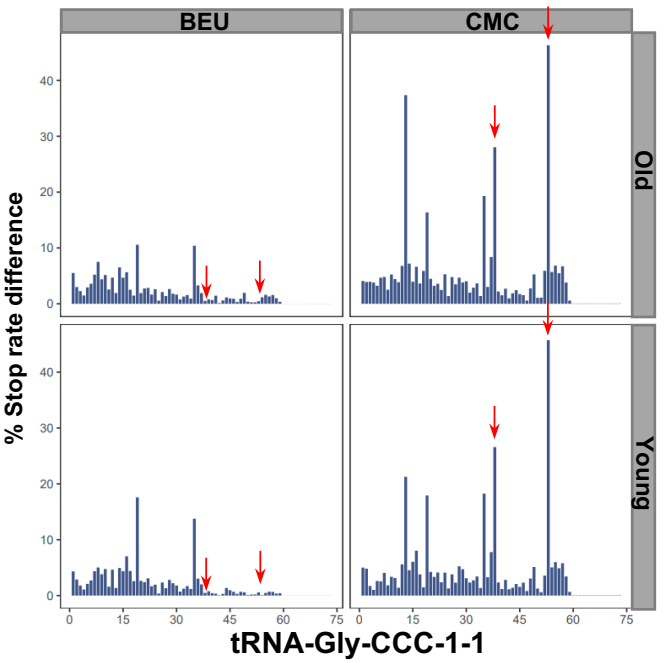
BEU
CMC
Old
Young
% Stop rate difference
0
10
20
30
40
0
15
30
45
60
75
tRNA-Gly-CCC-1-1

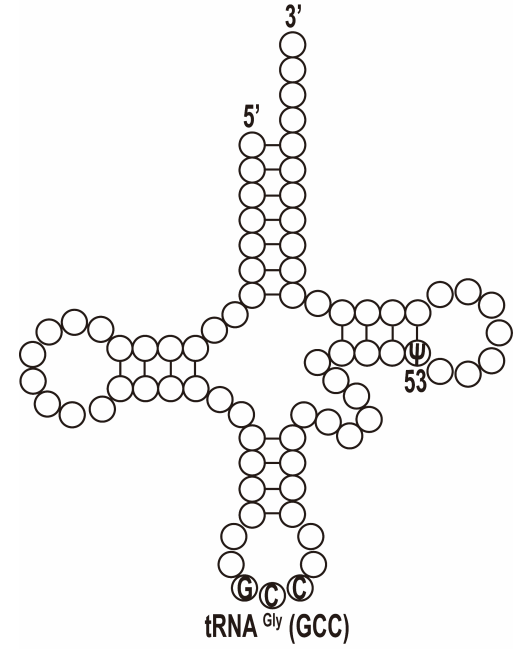
3'
5'
Ψ
53
G
C
C
tRNA Gly (GCC)

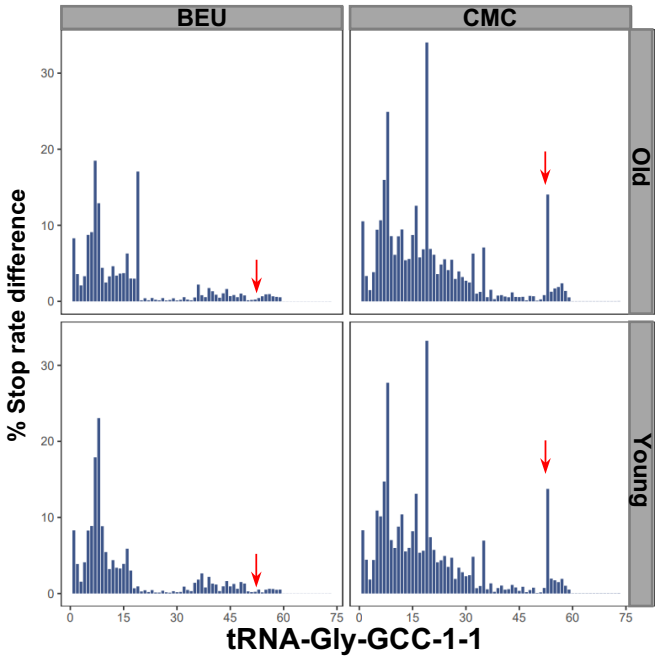
BEU
CMC
Old
Young
% Stop rate difference
0
10
20
30
0
15
30
45
60
75
tRNA-Gly-GCC-1-1

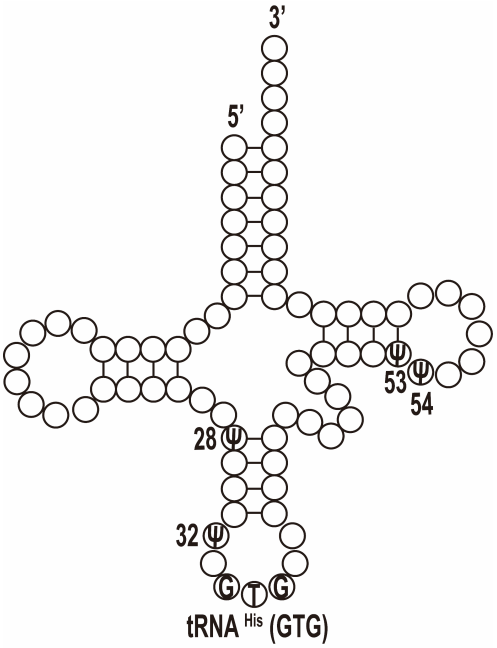
3'
5'
53
54
28
32
G T G
tRNA His (GTG)

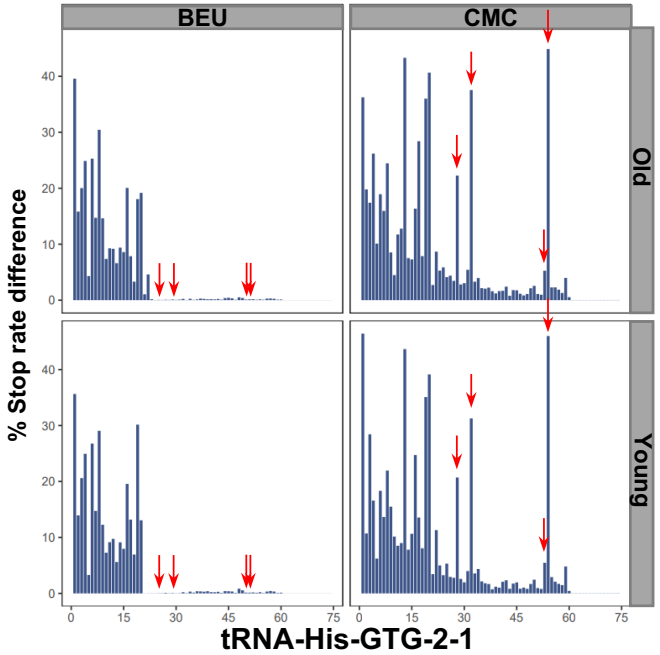
BEU
CMC
Old
Young
% Stop rate difference
tRNA-His-GTG-2-1

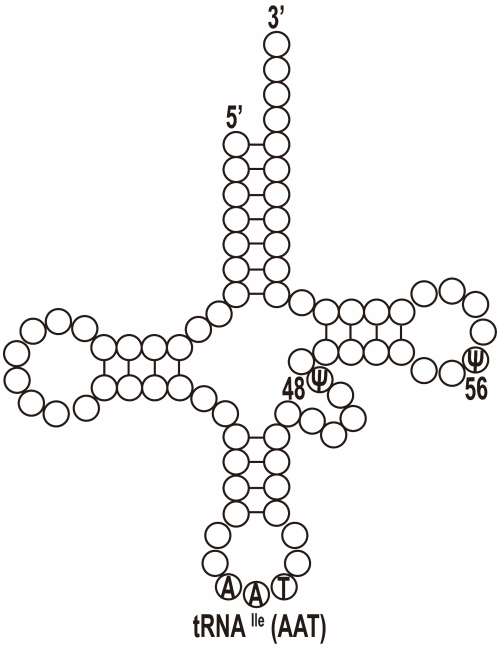
3'
5'
48
56
A A T
tRNA Ile (AAT)

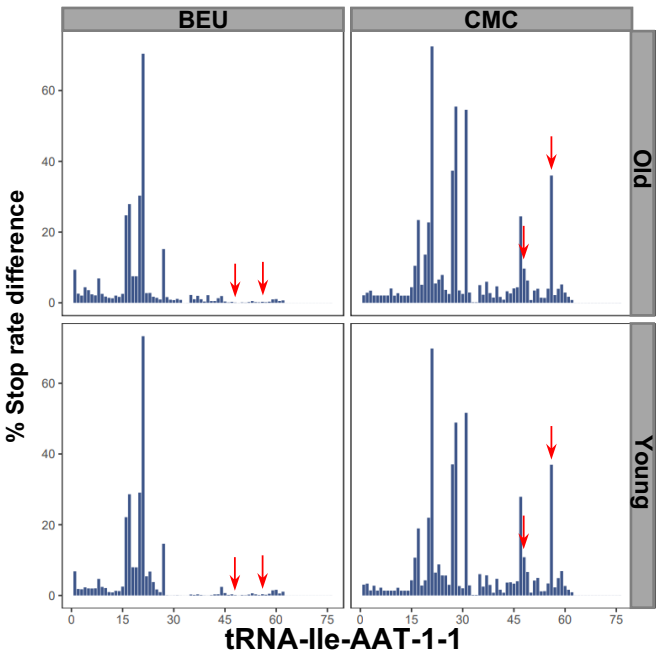
BEU
CMC
Old
Young
% Stop rate difference
tRNA-Ile-AAT-1-1

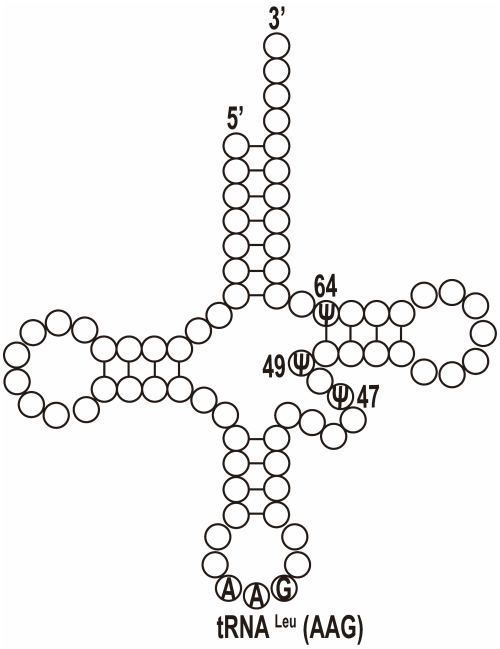
3'
5'
64
49
47
A A G
tRNA Leu (AAG)

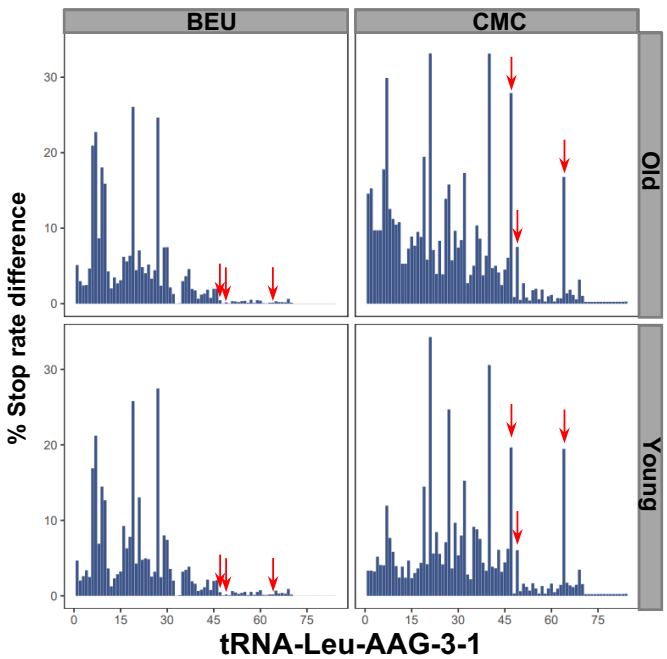
BEU
CMC
Old
Young
% Stop rate difference
tRNA-Leu-AAG-3-1

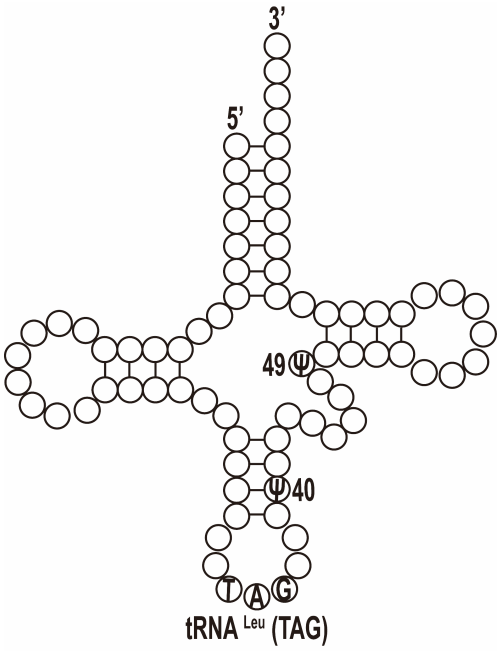
3'
5'
49Ψ
Ψ40
TAG
tRNA Leu (TAG)

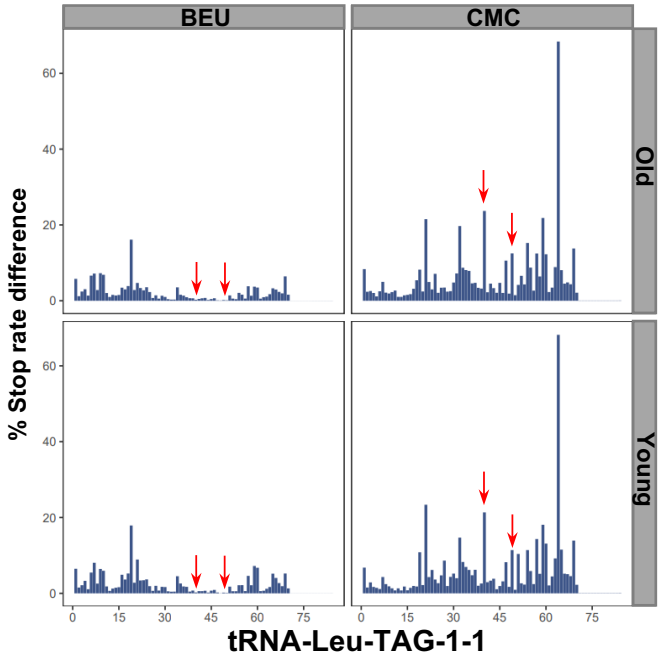
BEU
CMC
Old
Young
% Stop rate difference
tRNA-Leu-TAG-1-1

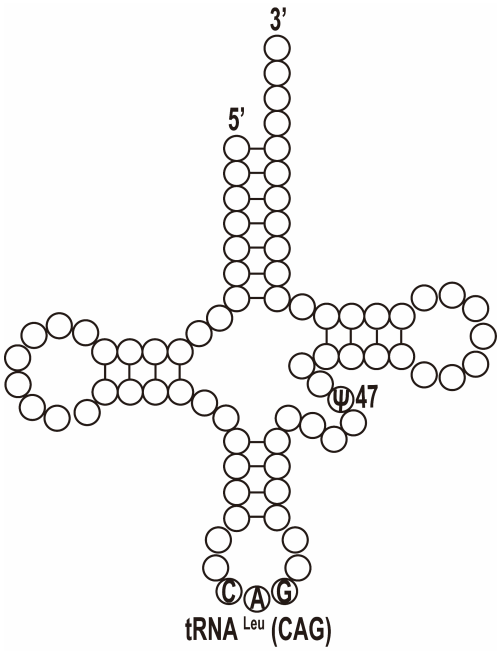
3'
5'
Ψ47
CAG
tRNA Leu (CAG)

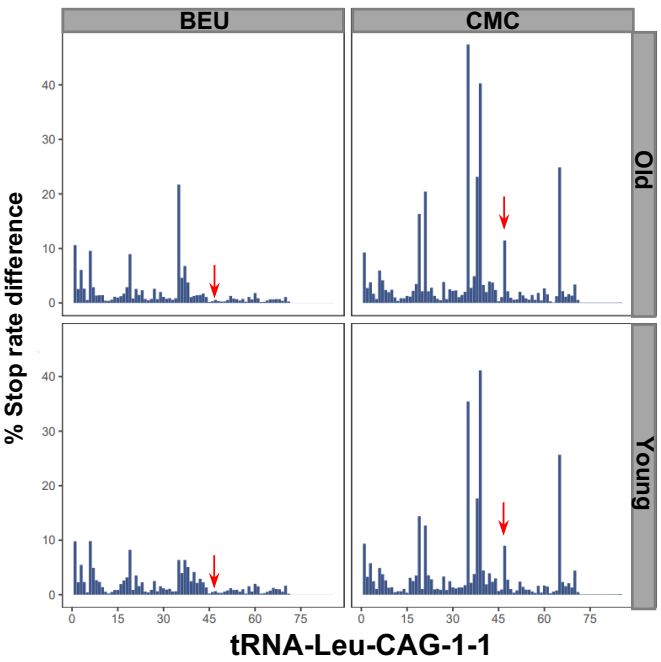
BEU
CMC
Old
Young
% Stop rate difference
tRNA-Leu-CAG-1-1

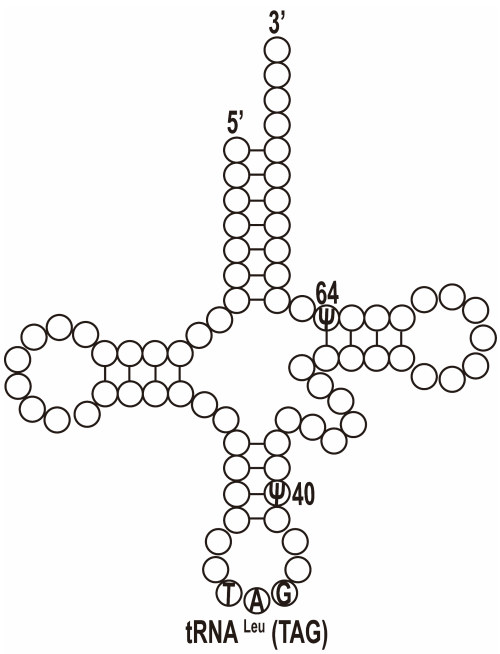
3'
5'
64Ψ
Ψ40
TAG
tRNA Leu (TAG)

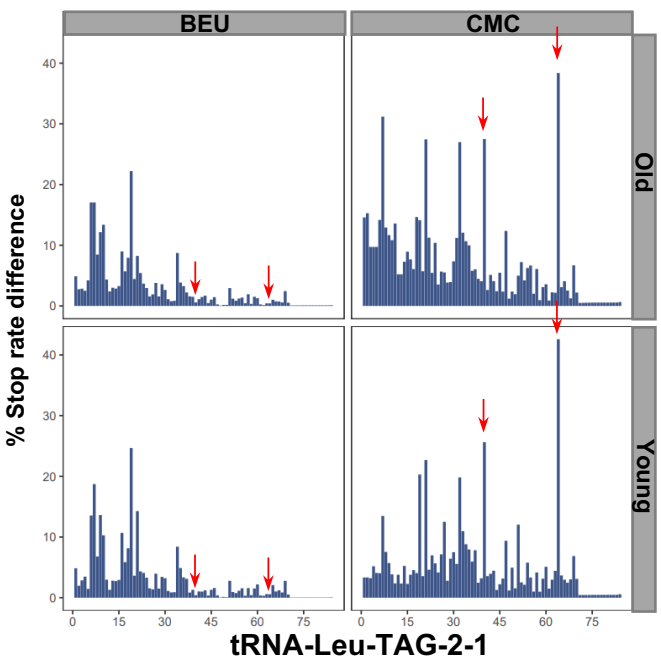
BEU
CMC
Old
Young
% Stop rate difference
tRNA-Leu-TAG-2-1

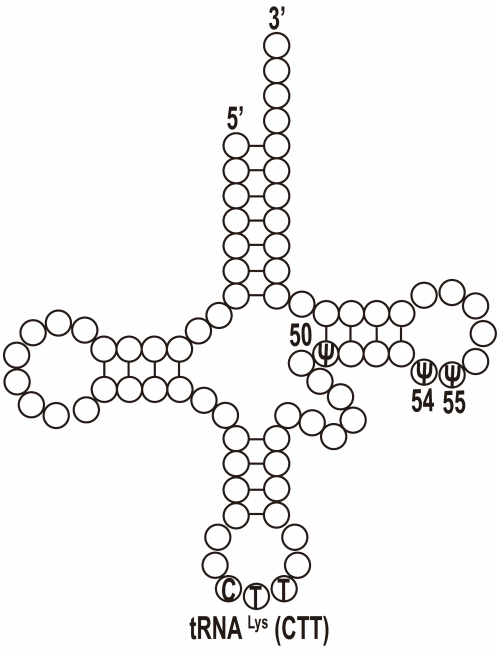
3'
5'
50
54
55
C
T
T
tRNA Lys (CTT)

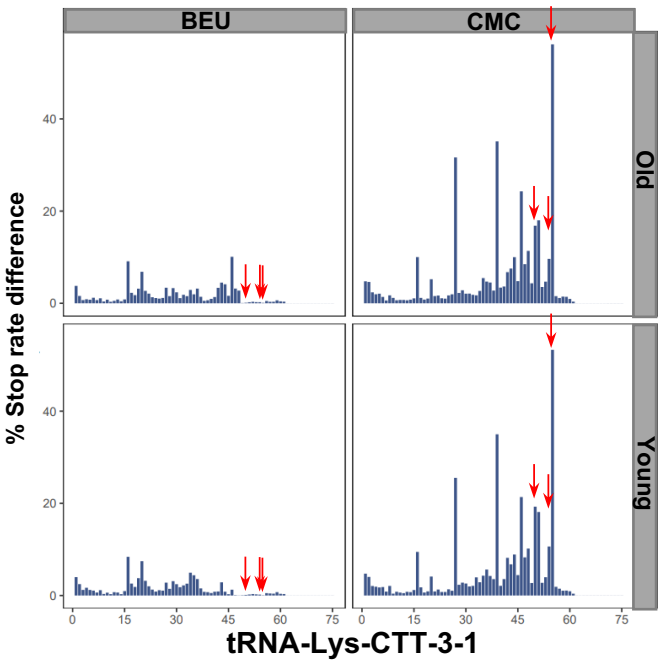
BEU
CMC
Old
Young
% Stop rate difference
0
20
40
0
15
30
45
60
75
tRNA-Lys-CTT-3-1

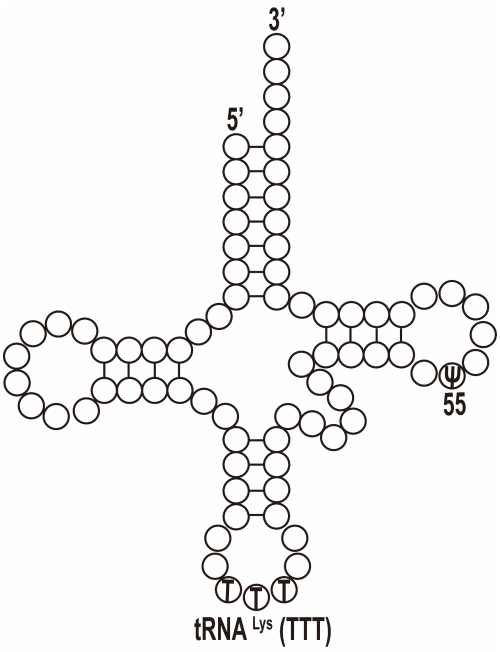
3'
5'
55
T
T
T
tRNA Lys (TTT)

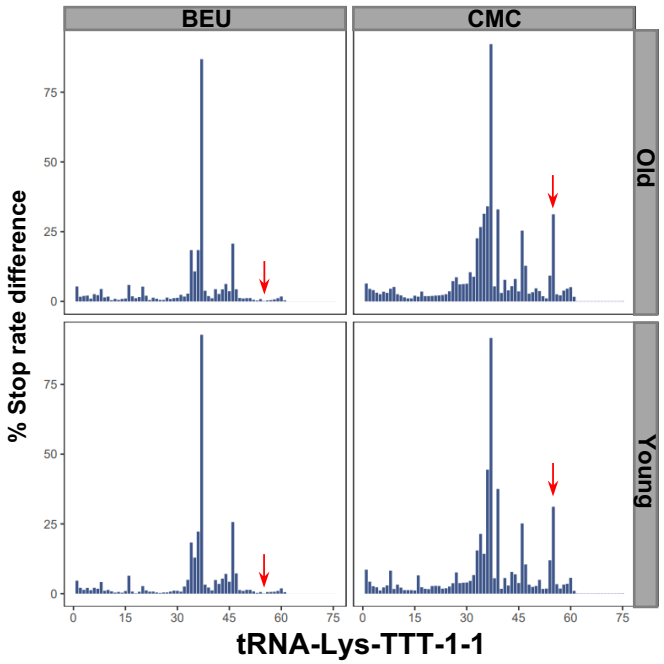
BEU
CMC
Old
Young
% Stop rate difference
0
25
50
75
0
15
30
45
60
75
tRNA-Lys-TTT-1-1

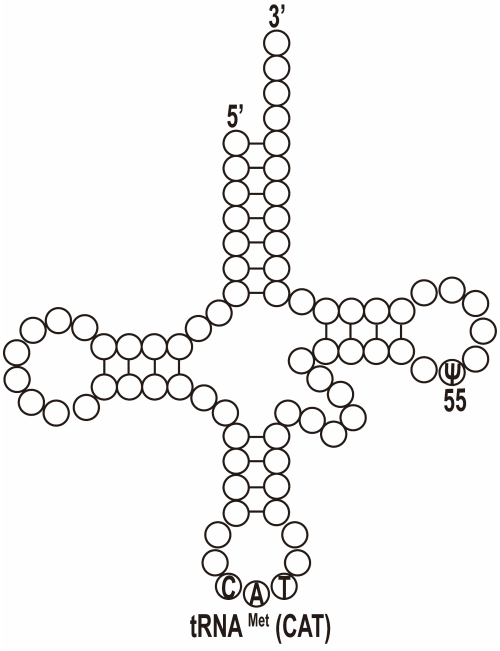
3'
5'
55
C
A
T
tRNA Met (CAT)

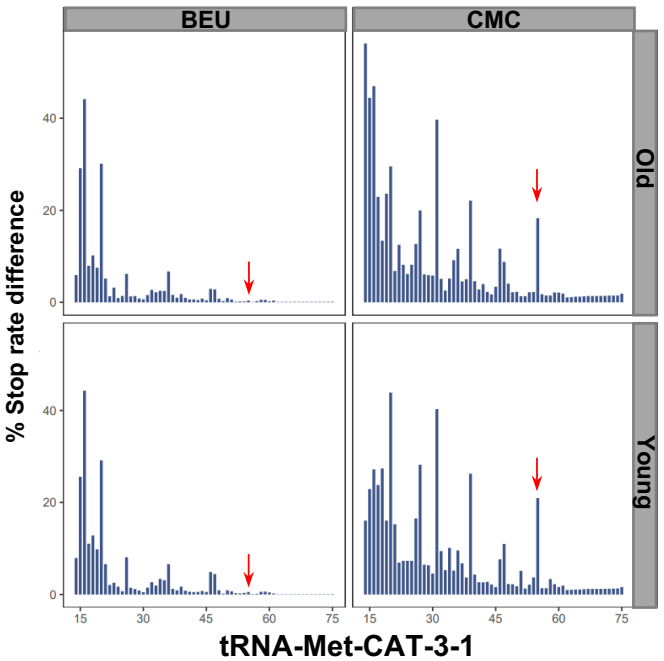
BEU
CMC
Old
Young
% Stop rate difference
0
20
40
15
30
45
60
75
tRNA-Met-CAT-3-1

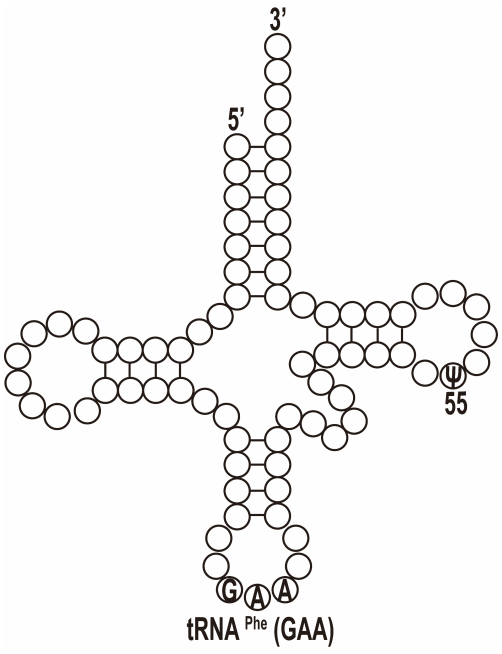
3'
5'
Ψ
55
G
A
A
tRNA Phe (GAA)

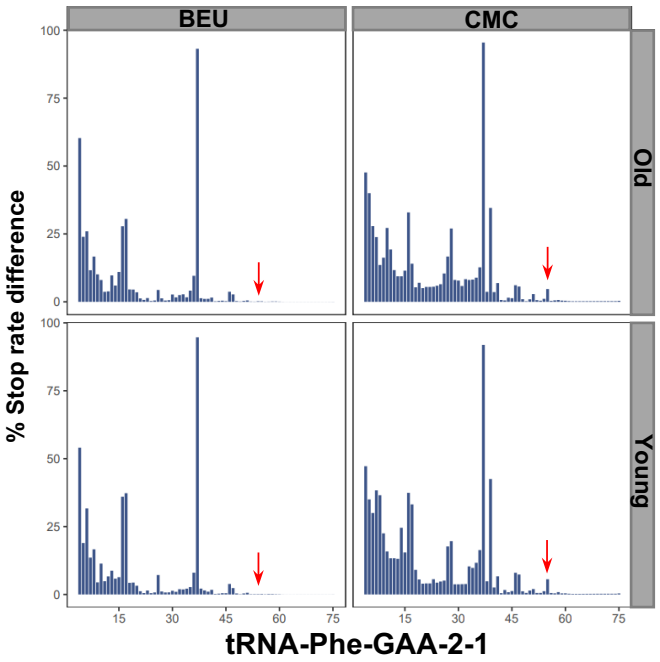
BEU
CMC
Old
Young
% Stop rate difference
tRNA-Phe-GAA-2-1

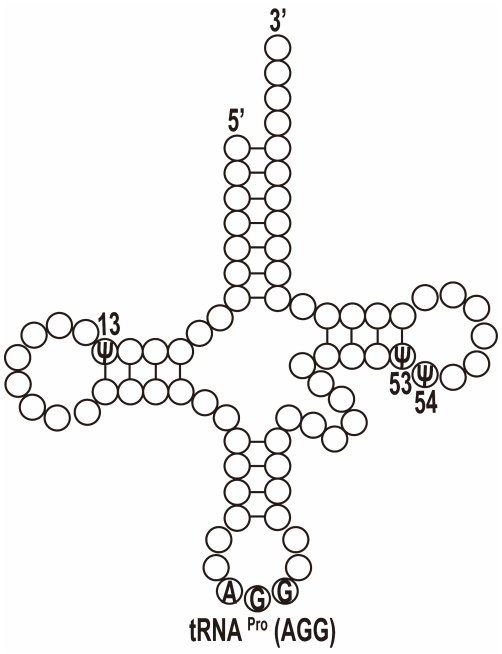
3'
5'
13
Ψ
53
Ψ
54
A
G
G
tRNA Pro (AGG)

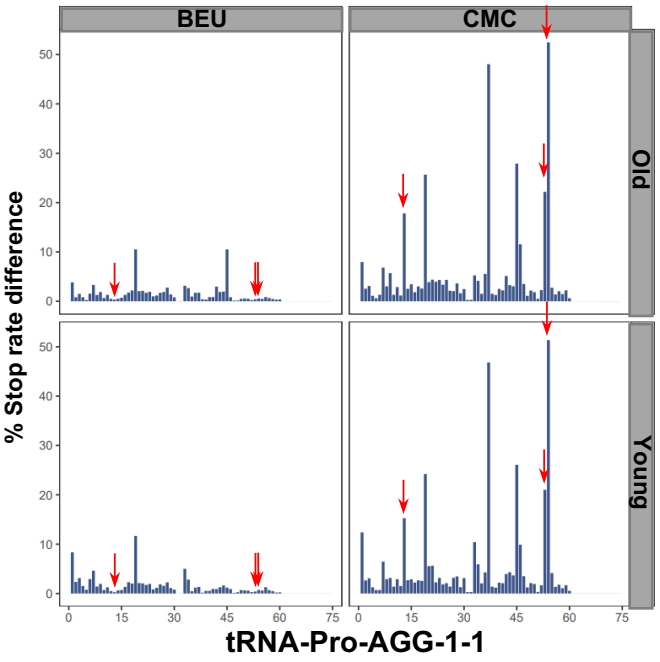
BEU
CMC
Old
Young
% Stop rate difference
tRNA-Pro-AGG-1-1

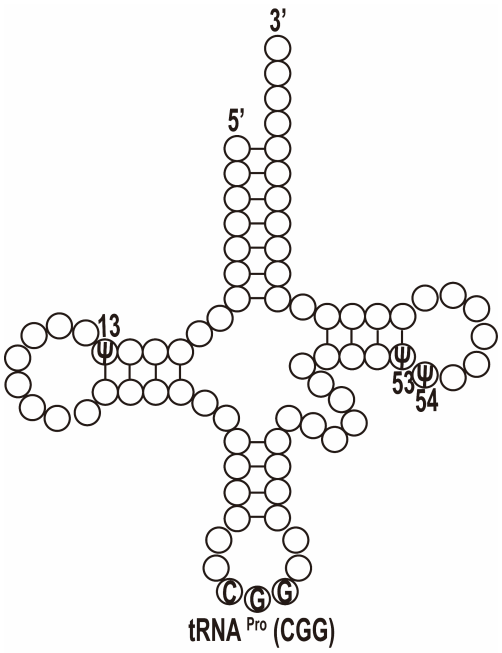
3'
5'
13
Ψ
53
Ψ
54
C
G
G
tRNA Pro (CGG)

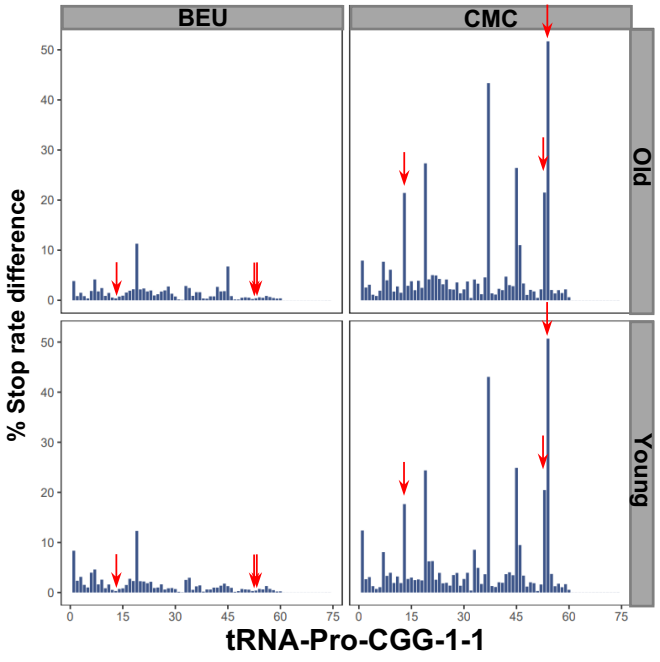
BEU
CMC
Old
Young
% Stop rate difference
tRNA-Pro-CGG-1-1

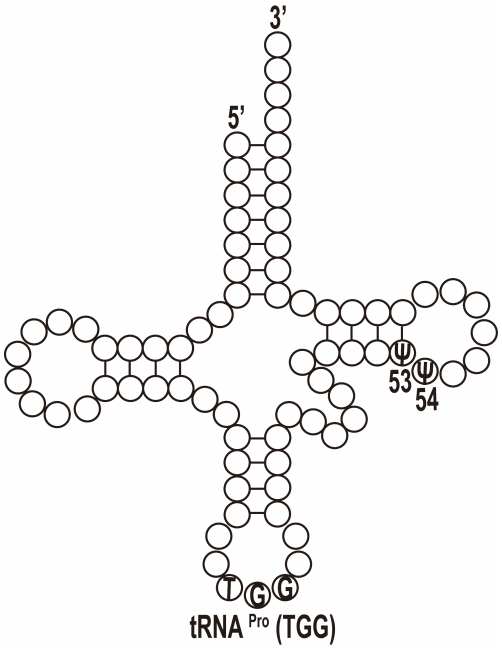
3'
5'
Ψ53
Ψ54
TGG
tRNA Pro (TGG)

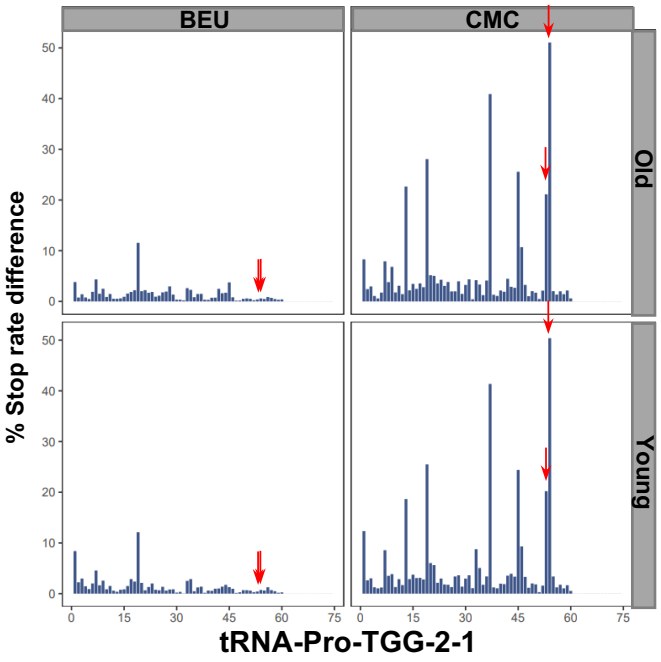
BEU
CMC
Old
Young
% Stop rate difference
tRNA-Pro-TGG-2-1

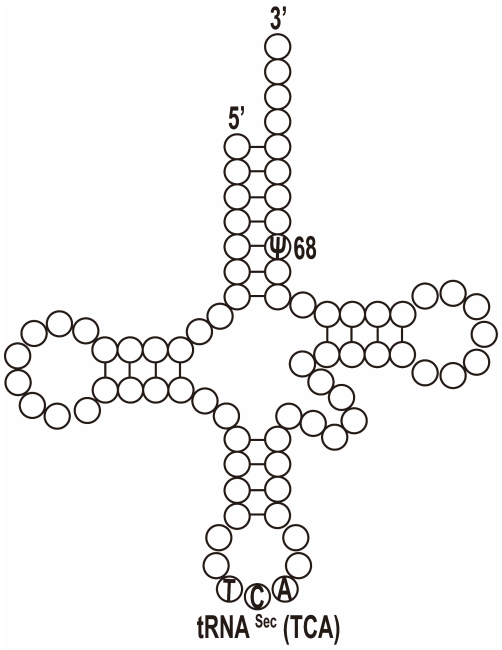
3'
5'
Ψ68
TCA
tRNA Sec (TCA)

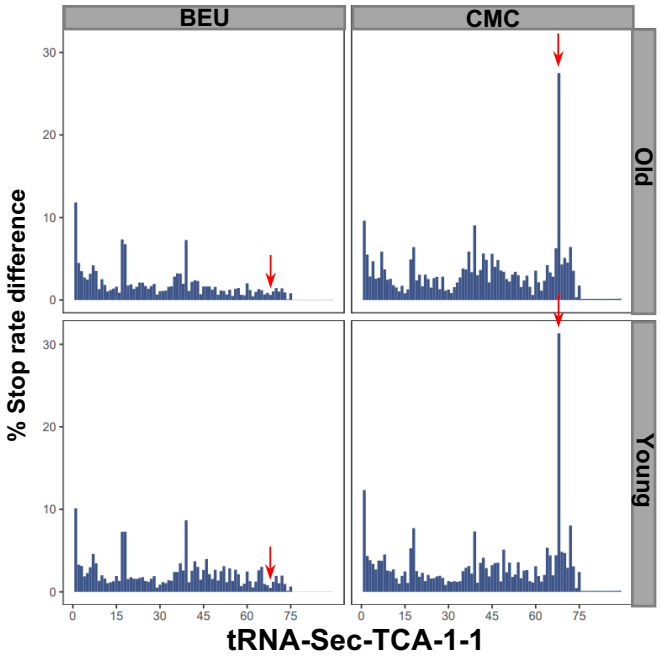
BEU
CMC
Old
Young
% Stop rate difference
tRNA-Sec-TCA-1-1

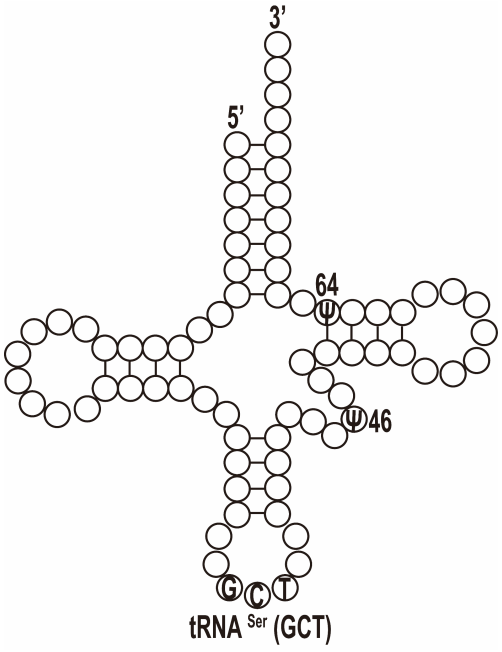
3'
5'
64
Ψ
Ψ46
GCT
tRNA Ser (GCT)

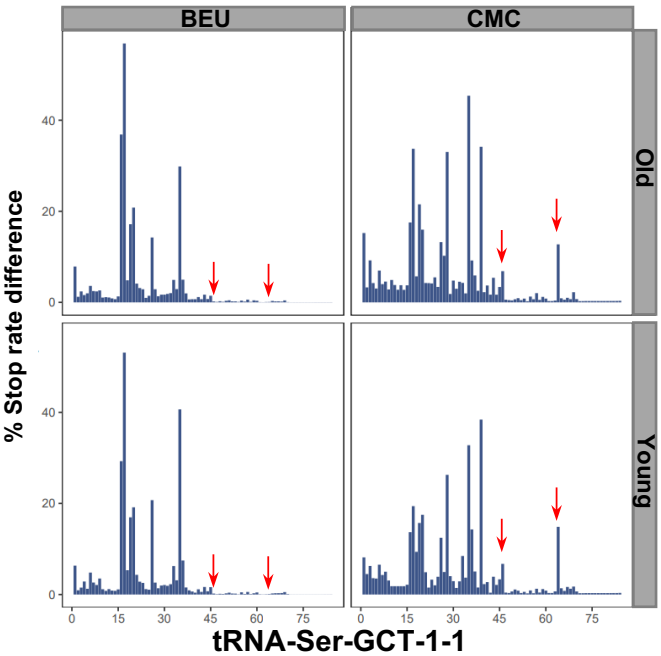
BEU
CMC
Old
Young
% Stop rate difference
tRNA-Ser-GCT-1-1

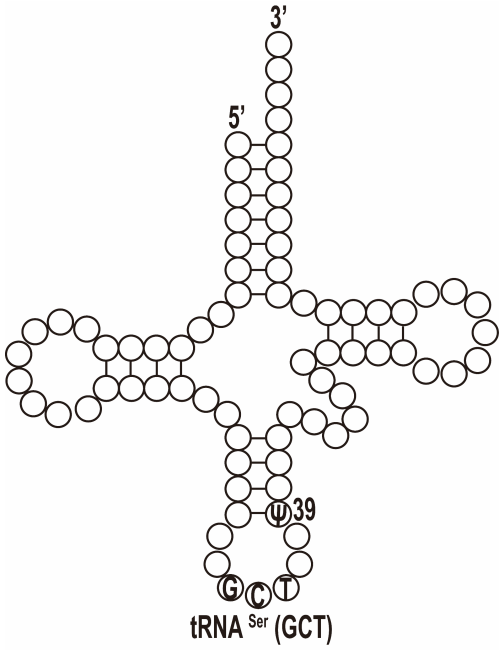
3'
5'
Ψ39
G C T
tRNA Ser (GCT)

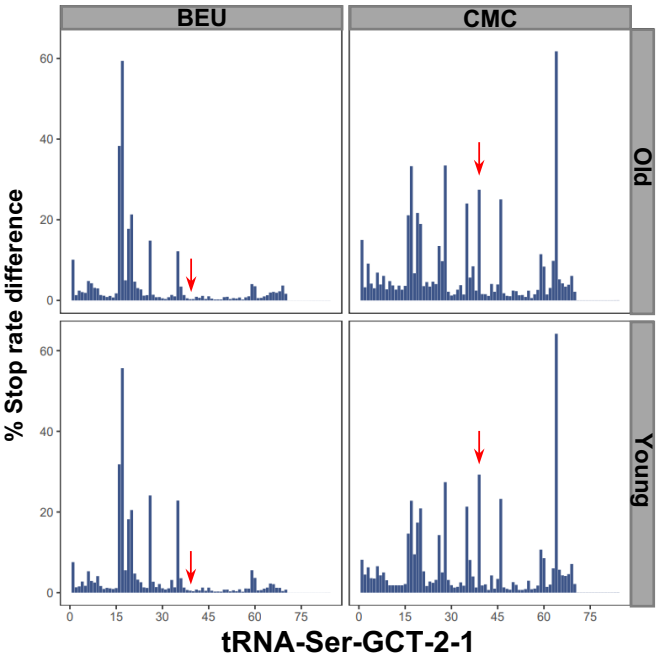
BEU
CMC
Old
Young
% Stop rate difference
0
20
40
60
0 15 30 45 60 75
tRNA-Ser-GCT-2-1

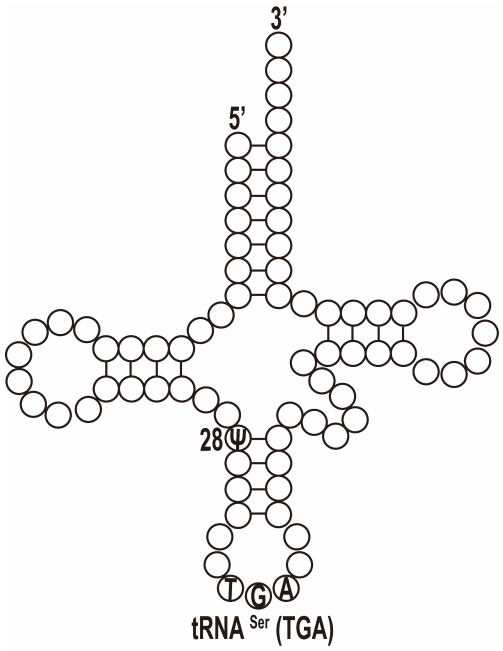
3'
5'
28Ψ
T G A
tRNA Ser (TGA)

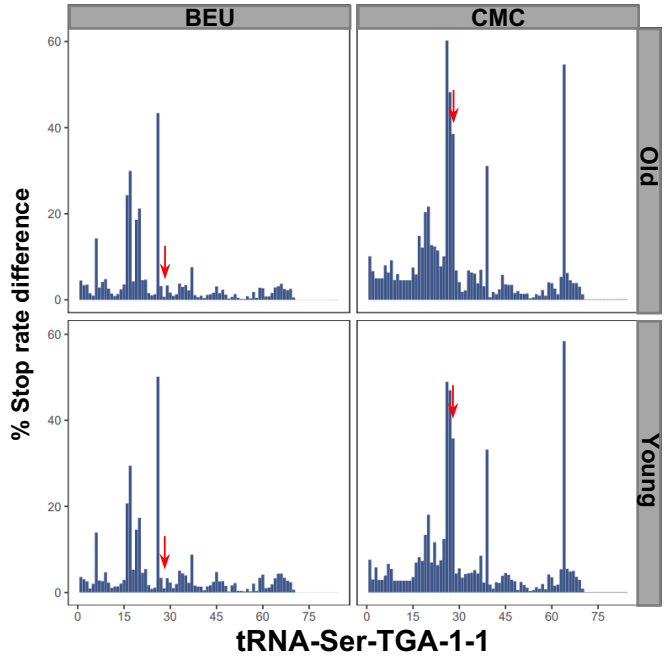
BEU
CMC
Old
Young
% Stop rate difference
0
20
40
60
0 15 30 45 60 75
tRNA-Ser-TGA-1-1

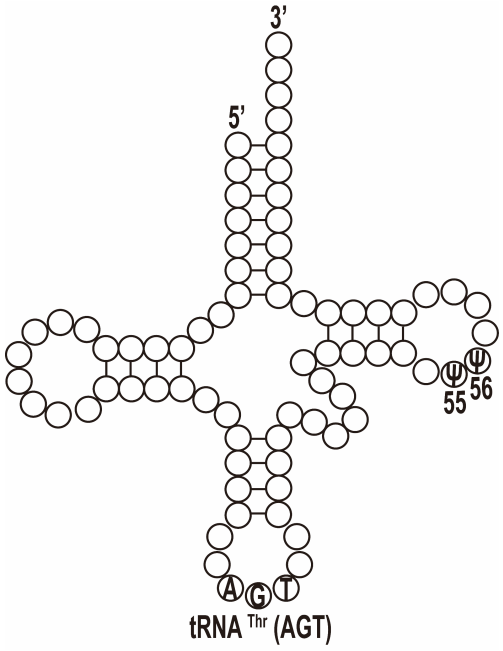
3'
5'
Ψ55
Ψ56
A G T
tRNA Thr (AGT)

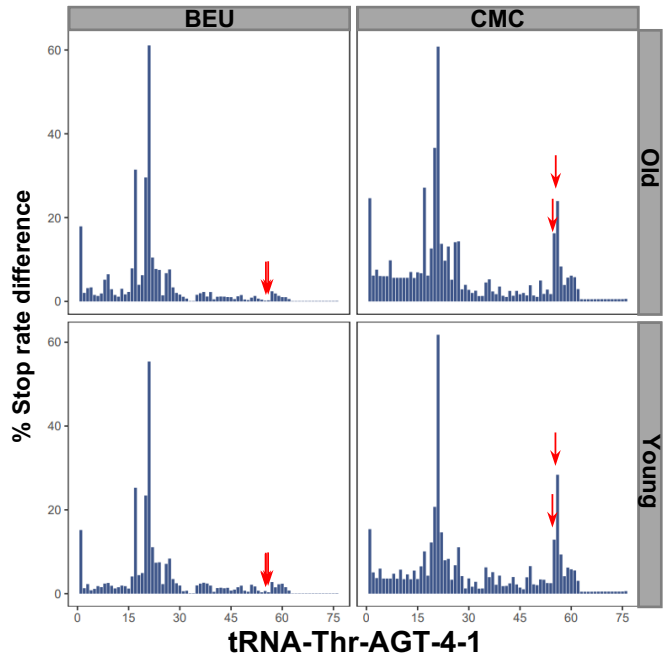
BEU
CMC
Old
Young
% Stop rate difference
0
20
40
60
0 15 30 45 60 75
tRNA-Thr-AGT-4-1

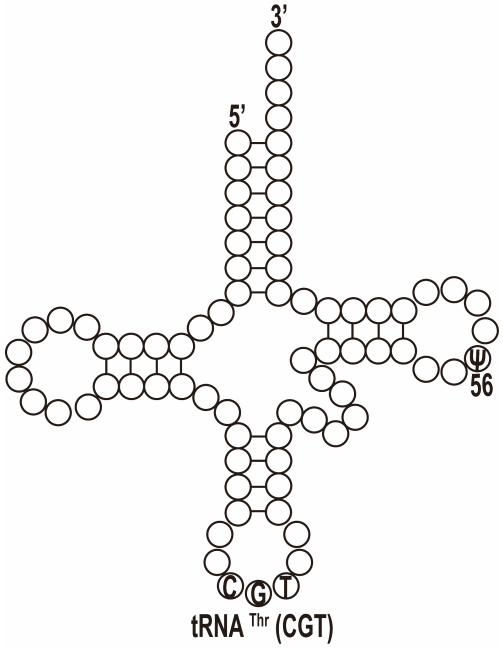
3'
5'
Ψ
56
C
G
T
tRNA Thr (CGT)

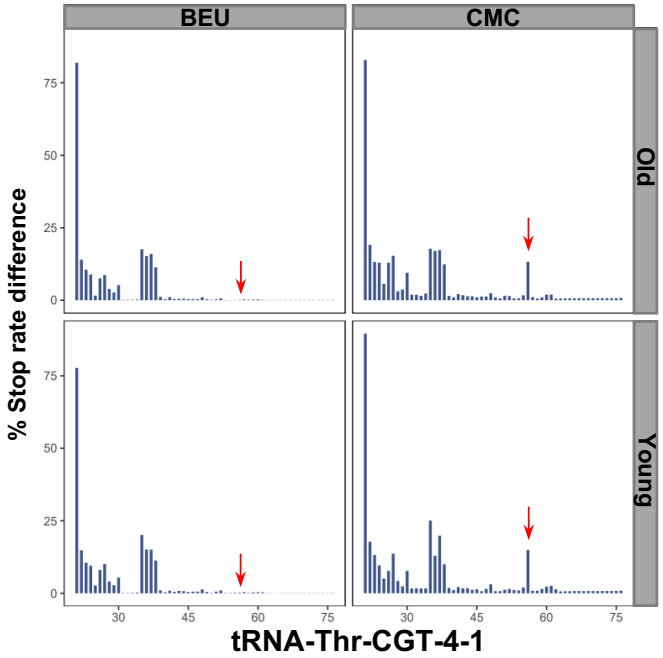
BEU
CMC
Old
Young
% Stop rate difference
tRNA-Thr-CGT-4-1

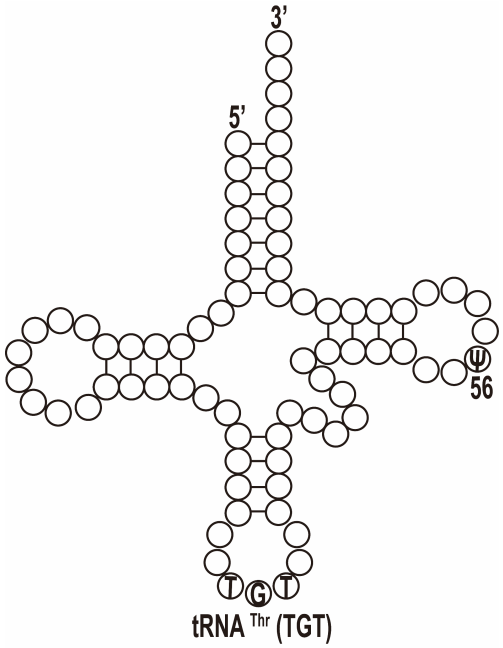
3'
5'
Ψ
56
T
G
T
tRNA Thr (TGT)

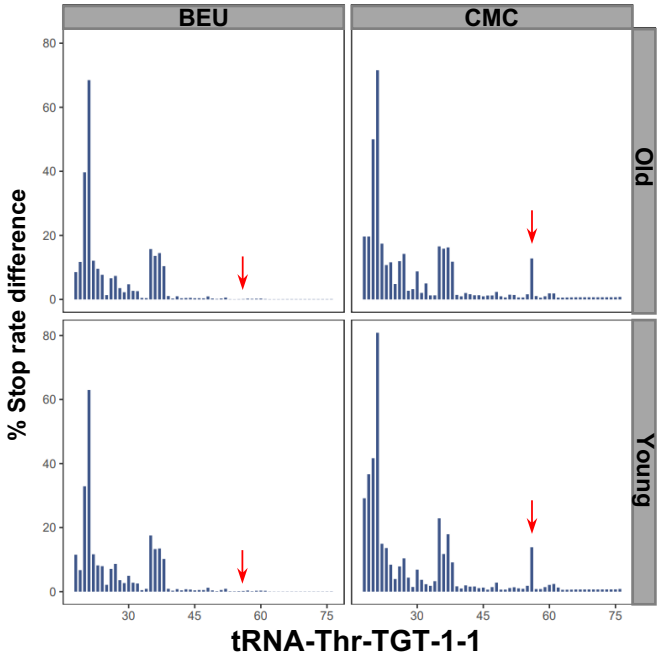
BEU
CMC
Old
Young
% Stop rate difference
tRNA-Thr-TGT-1-1

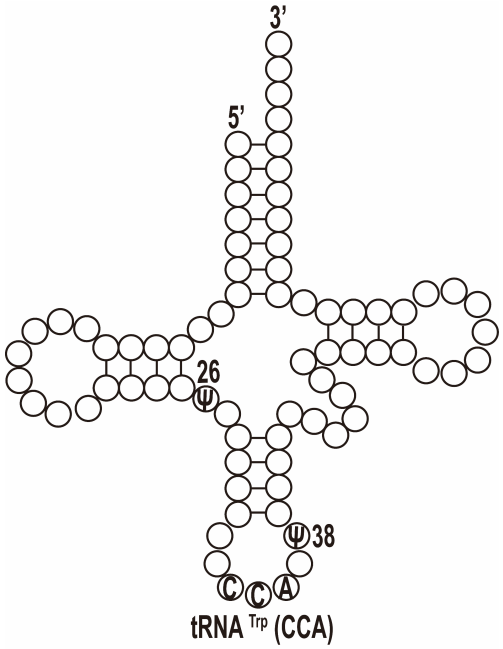
3'
5'
26
Ψ
Ψ38
C
C
A
tRNA Trp (CCA)

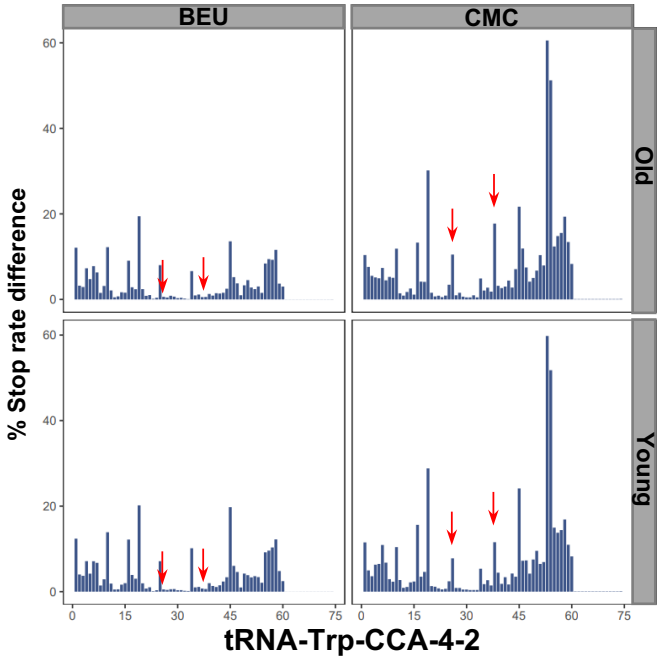
BEU
CMC
Old
Young
% Stop rate difference
tRNA-Trp-CCA-4-2

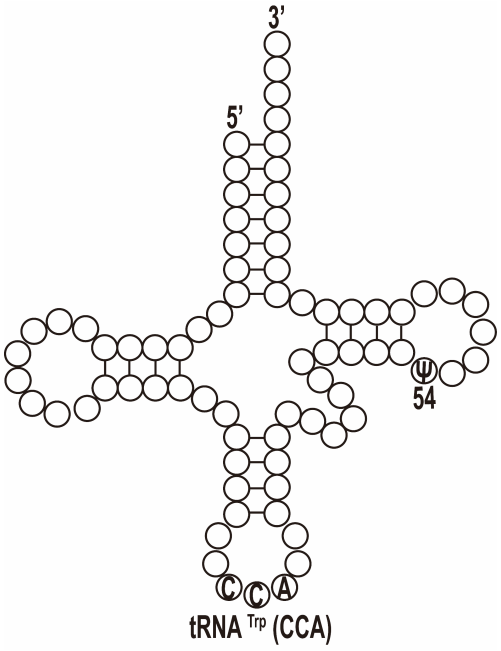
3'
5'
Ψ
54
C C A
tRNA Trp (CCA)

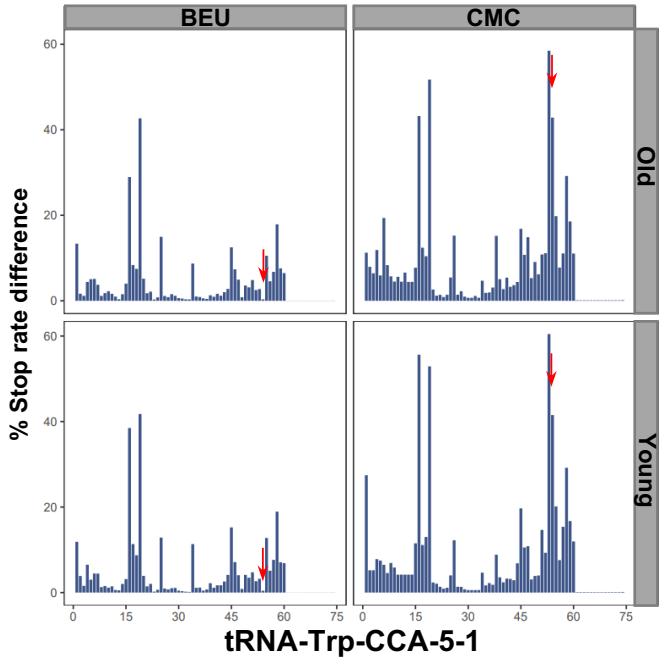
BEU
CMC
Old
Young
% Stop rate difference
tRNA-Trp-CCA-5-1

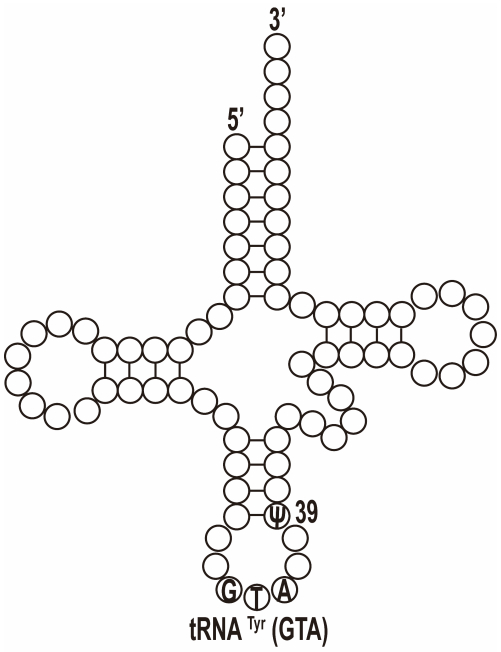
3'
5'
Ψ 39
G T A
tRNA Tyr (GTA)

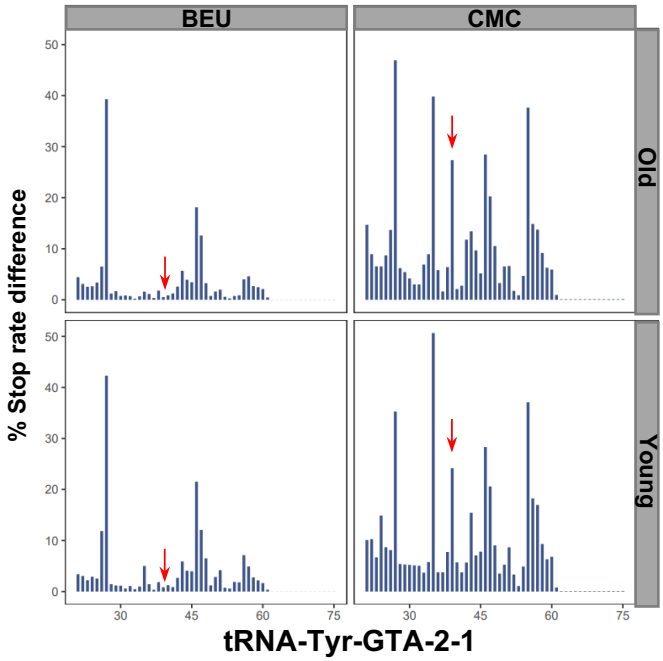
BEU
CMC
Old
Young
% Stop rate difference
tRNA-Tyr-GTA-2-1

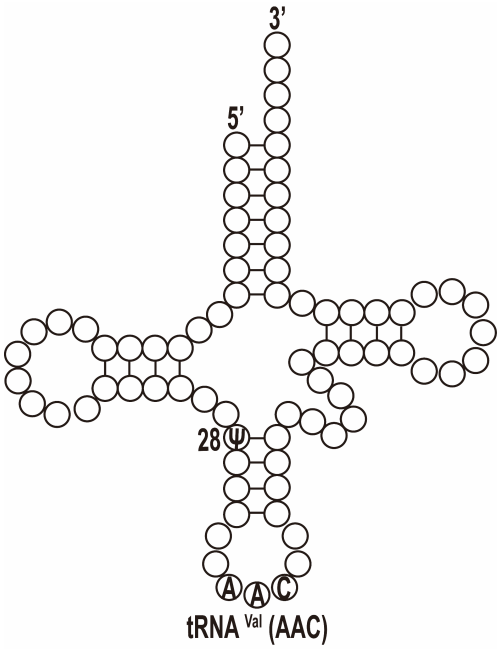
3'
5'
28 Ψ
A A C
tRNA Val (AAC)

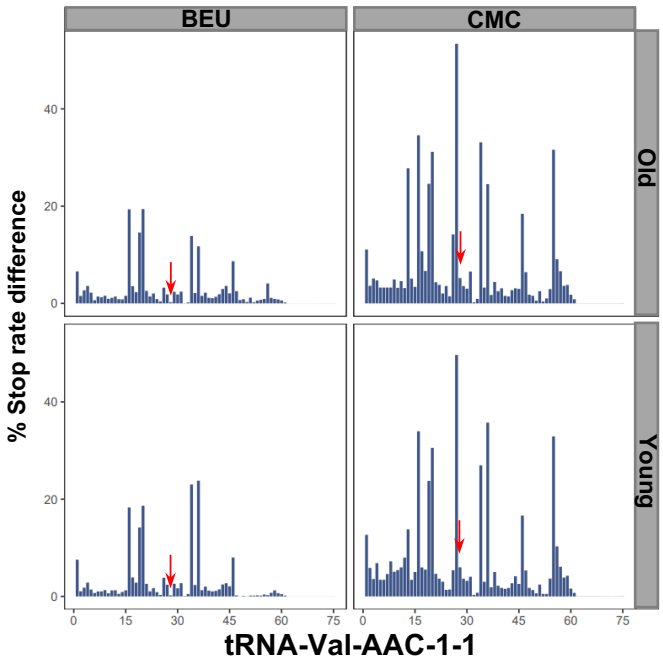
BEU
CMC
Old
Young
% Stop rate difference
tRNA-Val-AAC-1-1

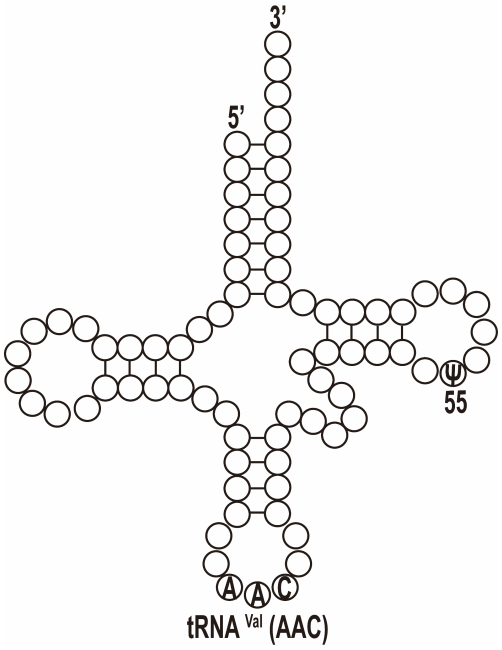
3'
5'
Ψ
55
A
A
C
tRNA Val (AAC)

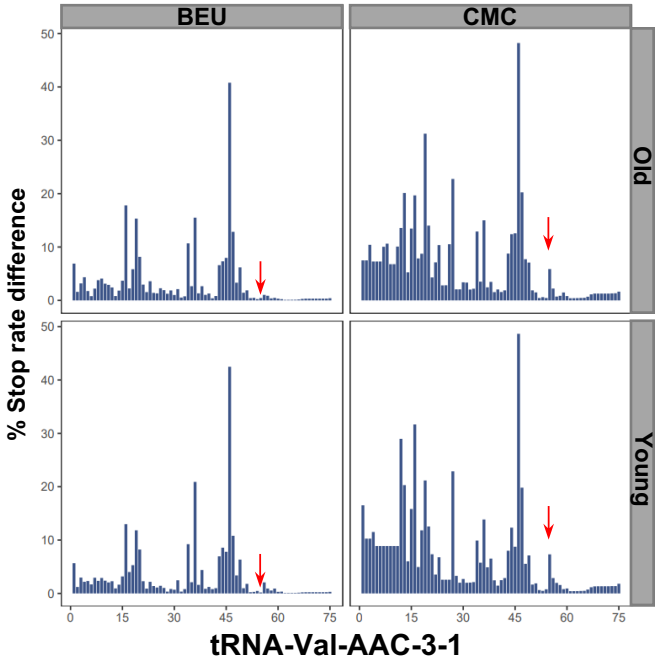
BEU
CMC
Old
Young
% Stop rate difference
0
10
20
30
40
50
0
15
30
45
60
75
tRNA-Val-AAC-3-1

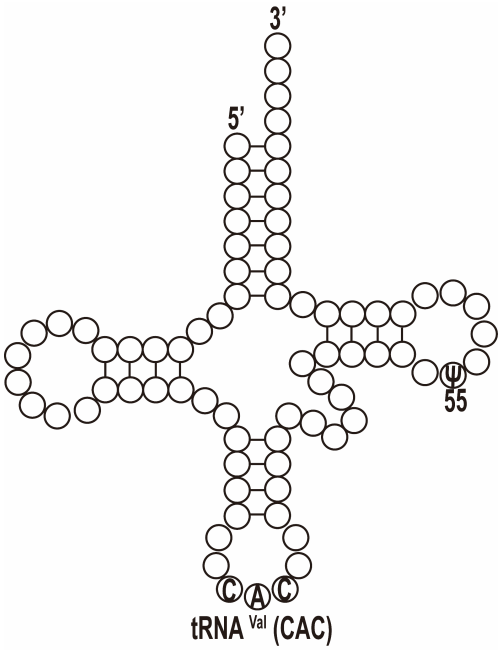
3'
5'
Ψ
55
C
A
C
tRNA Val (CAC)

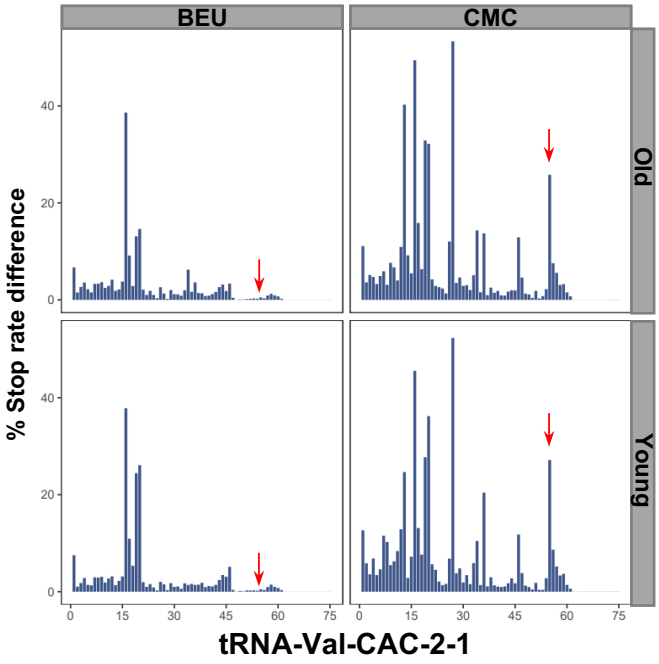
BEU
CMC
Old
Young
% Stop rate difference
0
20
40
0
15
30
45
60
75
tRNA-Val-CAC-2-1

Supplemental figure 3

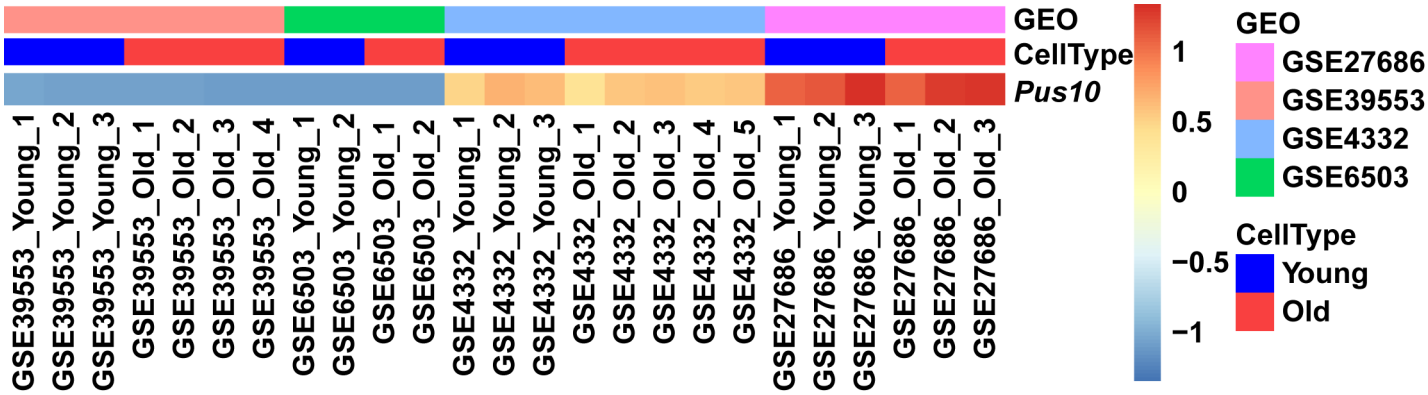

Supplemental figure 4

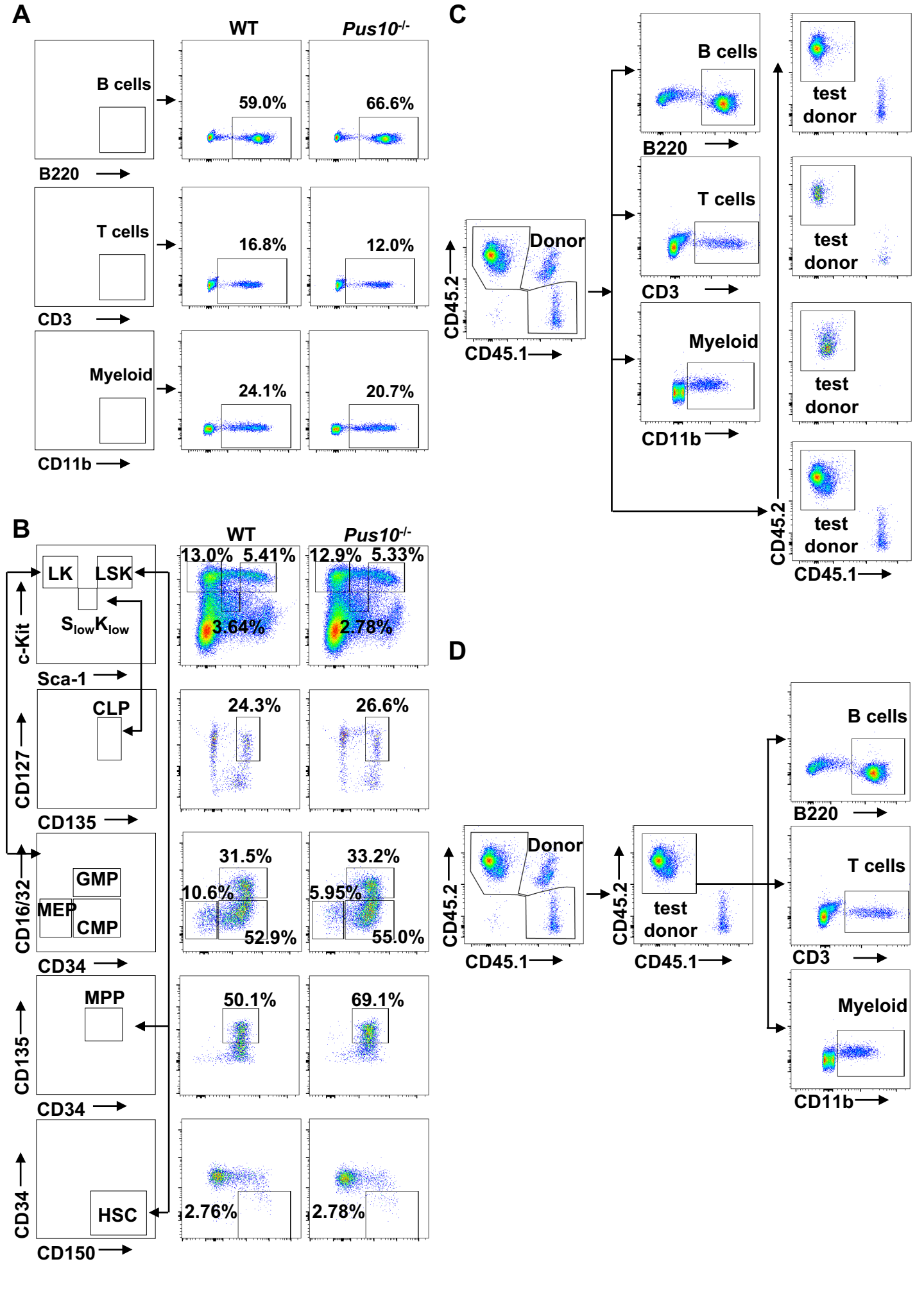

Uncropped blot Images for Fig.1A, Fig.3C,D,E,F and Fig.4B.

For Fig. 1A

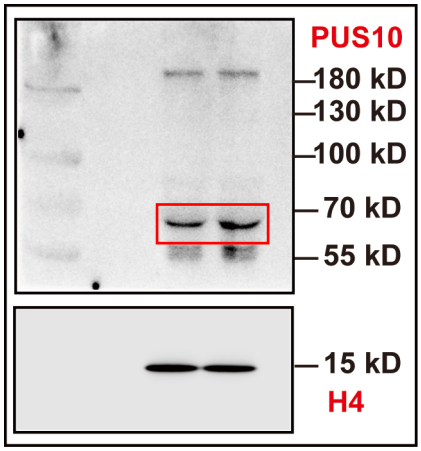

For Fig. 3E

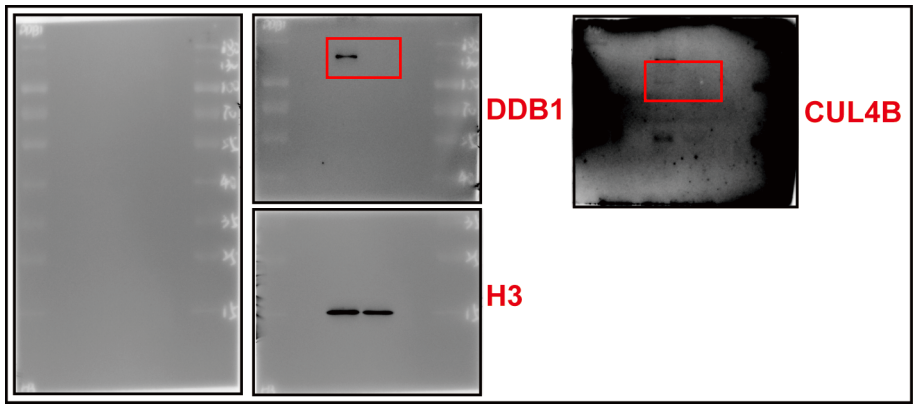

For Fig. 3C

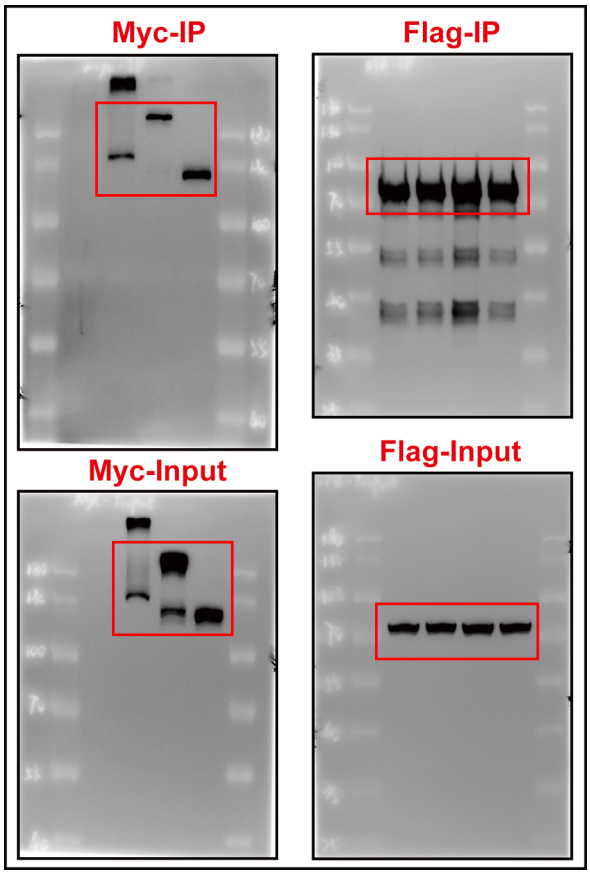

For Fig. 3D

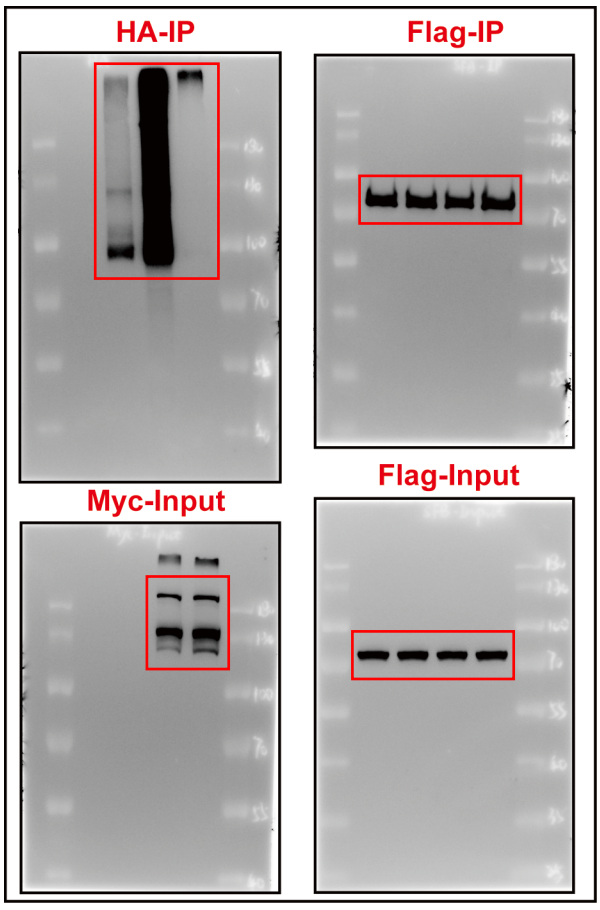

For Fig. 3F

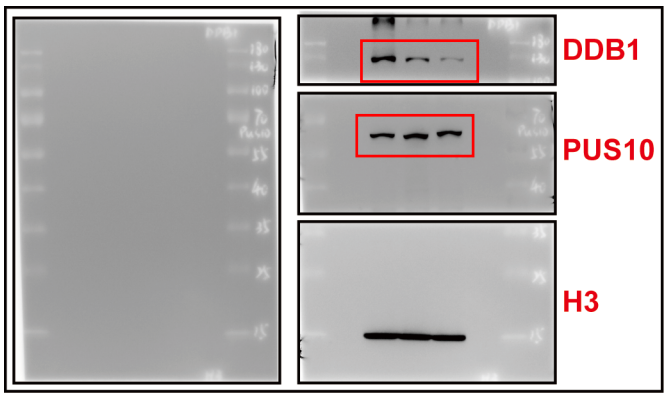

For Fig. 4B

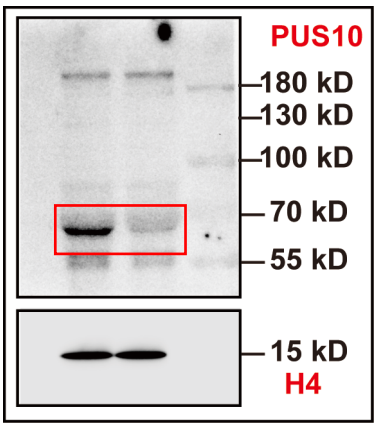

Uncropped blot Images for Supplemental Fig.1A

For Supplemental. Fig. 1A